

# Synchronization defect lines

Andrei Goryachev<sup>1</sup>, Hugues Chaté<sup>2</sup>, and Raymond Kapral<sup>1</sup>

<sup>1</sup>*Chemical Physics Theory Group, Department of Chemistry, University of Toronto, Toronto, ON M5S 3H6, Canada*

<sup>2</sup>*CEA — Service de Physique de l'Etat Condensé, Centre d'Etudes de Saclay, 91191 Gif-sur-Yvette, France*

Spatially distributed reaction-diffusion media where the local dynamics exhibits complex oscillatory or chaotic dynamics are investigated. Spiral waves in such complex-oscillatory or excitable media contain synchronization defect lines which separate domains of different oscillation phases and across which the phase changes by multiples of  $2\pi$ . Such synchronization defect lines arise from the need to reconcile the rotation period of a one-armed spiral wave with the oscillation period of the local dynamics. We analyse synchronization defect lines and show how to classify them and enumerate their types. In certain parameter regions the spatially distributed system exhibits line defect turbulence arising from the nucleation, growth and destruction of defect lines. The transitions to line defect turbulence may be characterized by power law behavior of order parameters and may be described as non-equilibrium phase transitions.

82.20.Wt, 05.40.+j, 05.60.+w, 51.10.+y

## I. INTRODUCTION

Reaction-diffusion media with local excitable or oscillatory elements support a variety of chemical waves which have been investigated extensively because of their relevance for a number of biological and chemical processes. [1–3] An important facet of nonlinear wave patterns, especially in oscillatory media, is that they organize the synchronization of local oscillations.

Many naturally occurring oscillations have complicated temporal patterns. Well known examples are mixed mode oscillations, period doubled oscillations or even chaotic oscillations. In this paper we describe chemical waves and pattern formation, as well as issues related to the synchronization of oscillations, in spatially distributed media where the local dynamics has a complicated periodic or chaotic structure. Our focus is on the existence, structure, stability and dynamics of spiral waves, which are one of the most commonly observed patterns in the laboratory and in nature.

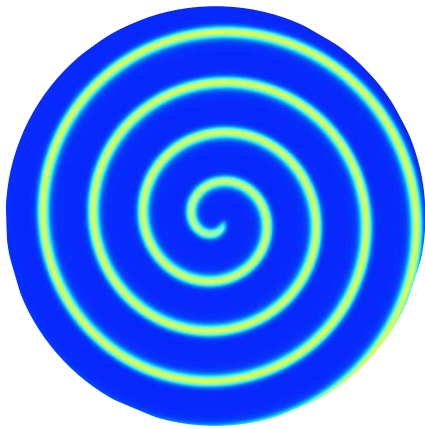


FIG. 1. A spiral wave in a disk-shaped oscillatory medium with no-flux boundary conditions and dynamics described by the Rössler reaction-diffusion equation in the period-1 regime. The  $c_z(\mathbf{r}, t)$  concentration field at a single time instant is displayed.

### *Simple spiral waves*

Pulse-like waves of excitation propagate in excitable media when the stable stationary state experiences a perturbation that exceeds a threshold. If the front of such a wave is broken the free ends will curl to form spiral waves which occupy the entire medium and persist as self-sustained patterns. In oscillatory media spiral waves arise from the diffusion-mediated synchronization of concentration oscillations in neighboring spatial points. A single spiral wave in an oscillatory medium is shown in Fig. 1.

The spiral wave in Fig. 1 is an example of a *simple* spiral wave. The concentration profile at time  $t$  of such a spiral wave can be obtained from a rotation of the concentration field at time  $t_0$  through some angle. The wave propagation can be considered to be a rotation of a stationary concentration profile around the spiral core. The local concentration varies periodically with time at arbitrary points of an oscillatory or excitable medium supporting a spiral wave. Although the mechanisms leading to the periodicity are different, in either case the local dynamics, represented as an orbit in concentration phase space, has the form of a simple closed loop which can be projected onto a two-dimensional phase plane without self-intersection. We shall call this period-1 dynamics to distinguish it from more complex-periodic patterns discussed below. In such a circumstance, it is always possible to introduce a phase variable  $\phi$  which uniquely parameterizes the orbit. The phase field  $\phi(\mathbf{r}, t)$  for a medium with a spiral wave contains a point topological phase defect [4] in the spiral core such that the integral

of the phase field gradient taken along any contour encircling the defect yields a non-zero value,

$$\frac{1}{2\pi} \oint \nabla\phi(\mathbf{r}, t) \cdot d\mathbf{l} = \pm n_t. \quad (1)$$

The signed integer  $n_t$  is the topological charge of the defect. The net topological charge of a medium with periodic boundary conditions is invariant; therefore, the defects are born or annihilated in pairs with opposite charge. In media with no-flux boundaries, the birth and destruction of defects may also occur on the boundaries; however, the sum of the topological charges of the medium and the boundary is constant. Although  $n_t$  can take on any integer value, we shall be concerned with commonly observed cases where only defects with  $n_t = \pm 1$  corresponding to one-armed spiral waves are stable. [5]

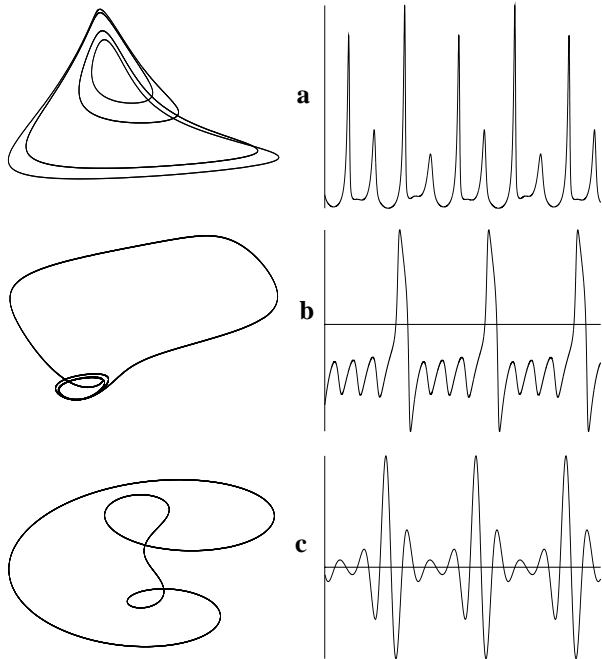


FIG. 2. Examples of complex-periodic oscillations: (a) a period-4 oscillation in a system with a period-doubling cascade; (b)  $1^3$  mixed-mode oscillation; (c) a period-4 oscillation on a torus. Left panels show phase portraits of orbits in a three-dimensional phase space while the right panels show the time series of a single dynamical variable.

### Complex oscillations

Together with simple period-1 dynamics, almost all known oscillatory reactions also display complex-periodic, aperiodic or chaotic behavior. [6] A complex-periodic oscillation is characterized by many peaks per full period if viewed as a time series of a single concentration variable and, in a suitably chosen concentration phase space, it corresponds to an orbit which loops sev-

eral times before it closes onto itself. Figure 2 shows examples of complex oscillations commonly seen in the laboratory and as the solutions of model reaction equations. Period doubled oscillations have period  $T_n \approx 2^n T_0$ , where  $T_0$  is the period of the orbit which spawned the period-doubling cascade, and are characterized by  $2^n$  loops in a phase space representation of the orbit (cf. Figs. 2(a) and (c)). One period of mixed mode  $\mathbf{n}^{\mathbf{m}}$  oscillations (MMO) consists of  $\mathbf{n}$  consecutive large-amplitude loops followed by  $\mathbf{m}$  small-amplitude loops (cf. Fig. 2(b)). We shall be concerned with situations where the local dynamics in a spatially-extended system exhibits such temporal patterns.

Complex-periodic dynamics is found also in excitable media. In some excitable systems re-excitation is possible before the previous relaxation cycle is complete but the response produced by the excitation is weaker. Since the execution of a smaller relaxation loop generally takes a shorter time, by the time the next excitation pulse arrives the medium has recovered completely and a normal response is produced. Then the entire pattern repeats. As a result, the system shows excitable behavior with alternating amplitude and the effective period of the local dynamics doubles. Such a phenomenon is observed, for example, in cardiac tissue [7] and is termed supernormal excitability. To illustrate this phenomenon consider a model excitable system of the form [8,9]

$$\begin{aligned} \frac{\partial u}{\partial t} &= \frac{1}{\varepsilon} u(1-u) \left( u - \frac{v+b}{a} - f(v) \right) + D\nabla^2 u, \\ \frac{\partial v}{\partial t} &= u - v, \\ f(v) &= \alpha \exp\left(-\frac{(v-v_0)^2}{\sigma^2}\right), \end{aligned} \quad (2)$$

where  $v$  is a non-diffusive variable and both  $u$  and  $v$  are functions of time and space. The excitable dynamics of system (2) consists of two fast and two slow stages. If displaced from the stable fixed point ( $u = 0, v = 0$ ) to the right of the unstable branch of the nullcline  $\dot{u} = 0$ , it quickly reaches upper stable branch  $u = 1$ . It follows this branch until  $v$  reaches sufficiently large values and then jumps to the lower stable branch  $u = 0$ , along which it slowly relaxes to the stationary state. To add a supernormal excitability to (2) the unstable branch of the nullcline  $\dot{u} = 0$  is modified by the function  $f(v)$  so that for suitably chosen parameters  $\alpha, \sigma$  and  $v_0$  it nearly touches the nullcline  $\dot{v} = 0$  (see Fig. 3). As a result, if another excitation is applied to the system (2) before it reaches the stationary state, it may execute a second, smaller excitable loop before finally returns to the stable state.

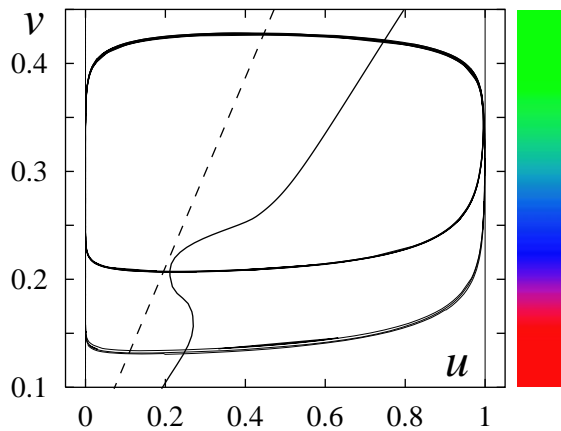


FIG. 3. Phase plane  $(u, v)$  plot of a  $\mathbf{1}^2$  type trajectory calculated at a point in a super-excitable medium. Two stable branches ( $u = 0, u = 1$ ) and one unstable branch of the nullcline  $\dot{u} = 0$  are shown as solid lines and the nullcline  $\dot{v} = 0$  by a dashed line.

The spatiotemporal dynamics of system (2) was studied in a one-dimensional array forced by an external pacemaker with varying period [9]. Non-trivial behavior consisting of mixed-mode wave forms  $\mathbf{1}^m$  was observed for certain values of the forcing. We will show below that instead of an external pacemaker one can use a spiral wave as a self-sustained source of excitation in the medium to induce such dynamics.

Complex or chaotic oscillations are quite common and expected to be generic for systems with more than two local scalar fields. Little is known about the spatiotemporal dynamics of media with such local oscillations. In the following, we show that in most circumstances the basic spatial patterns still exist and, in particular, spiral waves are easily observed; however, new features appear giving rise to qualitative changes in the overall synchronization of the medium.

To describe these systems a number of new terms need to be defined and some well-established notions, such as oscillation phase, require generalization. In Section II we describe the basic phenomenon, *synchronization defect lines*, which have been observed in experiments and numerical simulations. Next, a phase formalism is developed to describe these defect lines and demonstrate the necessity for their formation in complex-periodic media. The study of synchronization defect lines is continued in Sec. IV which considers a period-4 oscillatory medium in some detail. Section V develops an approach to the classification of defect lines and presents a complete solution to this problem for period-doubled media with period- $2^n$  local dynamics. The role of defect lines in the transition from complex-periodic to chaotic dynamics is considered in Sec. VI. Finally, our conclusions are summarized in Sec. VII.

## II. SYNCHRONIZATION DEFECT LINES

Consider a system described by the reaction-diffusion equation

$$\frac{\partial \mathbf{c}(\mathbf{r}, t)}{\partial t} = \mathbf{R}(\mathbf{c}(\mathbf{r}, t)) + D \nabla^2 \mathbf{c}(\mathbf{r}, t), \quad (3)$$

where  $\mathbf{c}(\mathbf{r}, t)$  is a vector of time-dependent concentrations at point  $\mathbf{r}$  in a two-dimensional physical space,  $D$  is the diffusion coefficient and the local kinetics is specified by the vector-valued function  $\mathbf{R}(\mathbf{c}(\mathbf{r}, t))$ . As a specific example of a reaction-diffusion system with complex local dynamics we take  $\mathbf{R}(\mathbf{c})$  to be given by the Rössler model [10] with  $R_x = -c_y - c_z$ ,  $R_y = c_x + A c_y$ ,  $R_z = c_x c_z - C c_z + B$ . The behavior of this system was investigated for  $C$  in the interval  $[2., 6.]$  with the other parameters fixed at  $A = B = 0.2$ . We observed that the spatially-distributed medium undergoes period-doubling bifurcations. Simulations designed to characterize the period-doubling transitions were performed on a disk-shaped domain ( $R = 256, D = 1.6$ ) with a single spiral wave in the center. [11,12] The spiral wave concentration profile in the period-1 regime was taken as the initial condition. The parameter  $C$  was gradually incremented and a long equilibration time was allowed for the dynamics to reach the new system state at each new value of  $C$ . This Rössler reaction-diffusion medium with a spiral wave undergoes a first period-doubling bifurcation at  $C = C_1^* \approx 3.03$ . Within the period-2 domain, the spiral wave acquires a global structure that differs from that in a simple periodic medium. Figure 4 shows the  $c_z(\mathbf{r}, t_0)$  concentration field at a single time instant  $t_0$ .

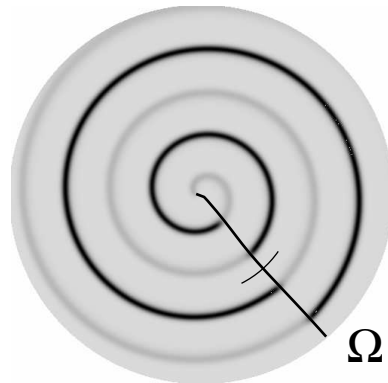


FIG. 4. Spiral wave in the Rössler medium with no-flux boundary conditions and period-2 local dynamics at  $C = 3.84$ . Concentration field  $c_z(\mathbf{r}, t)$  is shown as grey shades. The solid line depicts the  $\Omega$  curve. Dynamics on the small arc segment that transversally cuts the  $\Omega$  curve will be described below.

The most prominent feature of this spiral wave with period-2 local dynamics is the presence of a line, labeled  $\Omega$  in Fig. 4, which connects the spiral wave core to the boundary. Along this line the pattern is displaced by one wavelength. While the wave propagates, the dislocation line remains stationary and its position is traced

by the free ends of the propagating high-amplitude wave segments. The dislocation line is nearly straight with a gentle bend where it approaches the spiral wave core. The concentration time series at any two nearby points on opposite sides of this line are shifted in time relative to each other by one period of rotation of the spiral. The passage of a high-amplitude wave maximum through one observation point is synchronized with the passage of a low-amplitude maximum through the other and vice versa. We call this line a *synchronization defect line*. Two arbitrary states of the spiral wave evolution cannot be transformed into each other by simple rotation of the entire concentration field. After one turn of the spiral the high and low maxima interchange and it is only after two spiral revolutions that the concentration field is restored to its initial value.

Synchronization defect lines were studied also in the Willamowski-Rössler [13] reaction-diffusion system where period doubling in spiral wave dynamics was observed. [11] In this system the  $\Omega$  line connecting the spiral core to the medium boundary had a spiral geometry and slowly rotated with a frequency much smaller than that of the oscillation frequency. All of the other characteristic features of synchronization defect lines described above were the same as those seen in this reaction-diffusion model.

Synchronization defects are not confined to systems where the complex dynamics arises from period-doubling and were found also in the model system with super-normal excitability described earlier (cf. Eq. (2)) [14]. The parameters  $\alpha$  and  $\sigma$ , which control the size of the bell-shaped hump on the nullcline  $\dot{u} = 0$ , were varied to change the preference for formation of low-amplitude waves over high-amplitude waves. For small  $\alpha$  and  $\sigma$  the medium formed normal, high-amplitude spiral waves with  $\mathbf{1}^0$  local dynamics, while for large  $\alpha$  and  $\sigma$  the relaxation of excitation always took a short path and low-amplitude  $\mathbf{0}^1$  waves with a short wave length were observed. Complex-excitable dynamics was found in the parameter region between these domains. In this region the medium supports mainly aperiodic, stable spiral waves. Pure period-3 dynamics was found in a sub-domain of this region.

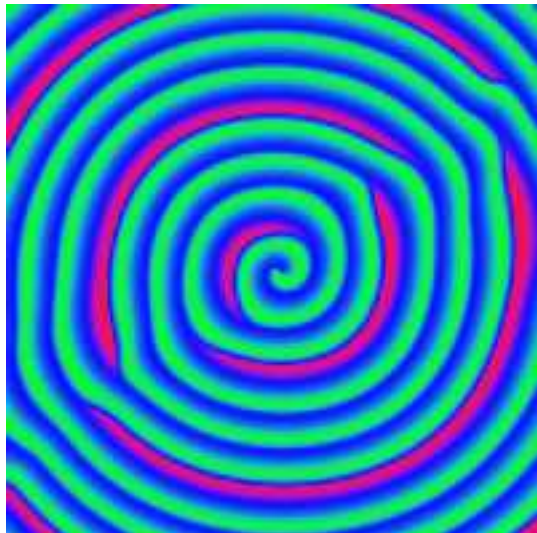


FIG. 5. Spiral wave with period-3 dynamics. Color-coding of the  $v$  field is indicated in Fig. 3.

Figure 5 shows a spiral wave in this period-3 parameter region. The entire concentration field slowly rotates around the spiral core with a constant angular velocity  $\omega$ . The period-3 dynamics is manifest in a coordinate frame centered at the spiral core and rotating with angular velocity  $\omega$ . Indeed, it takes three rotations of the spiral for the concentration field to return to itself. In Fig. 5 one clearly sees two dislocation lines emanating from the spiral wave core and subtending an angle of approximately  $180^\circ$ .

#### A. Experimental observations of defect lines

Synchronization defect lines have been observed experimentally in a spatially heterogeneous BZ reaction system consisting of thin (0.7 mm) layer of a Mn-catalyzed BZ reaction mixture with a monolayer of the surfactant-derivative of the ruthenium-bipyridil complex on its top [15]. Spiral waves were created by mechanical disruption of chemical waves spontaneously emerging at the dish boundaries and the dynamics of the waves on the surface of catalyst and in the bulk of the solution was monitored using fluorescence microscopy of reflected and transmitted light, respectively. Scroll waves, whose propagation on the surface and in the bulk showed no differences, were observed in a nitrogen atmosphere above the solution.

When the nitrogen atmosphere was replaced by air, the spiral on the surface developed collapsed wave segments with subthreshold amplitude which appear on fluorescent images as completely blank spaces. These collapsed segments, which are created at the tip of the spiral, propagate to the boundary as the wave unwinds from the tip. The scroll wave rotating in the underlying solution had uniform amplitude and, thus, propagation failure occurred only on the catalytic surface. The fragmented surface spiral wave preserved its integrity and free ends

of normal fragments exhibited no tendency to curl with formation of new spiral waves. In the initial stages of the evolution collapsed fragments were formed randomly and no order could be seen in the succession of the two types of wave front. However, with time the dynamics locked into the  $1^1$  regime with strict alternation of high- and low-amplitude waves so that the suprathreshold response on the surface occurred on every second passage of the wave front in the underlying solution. As a result the wave on the surface developed into the wavelength-doubled form shown in Fig. 6.

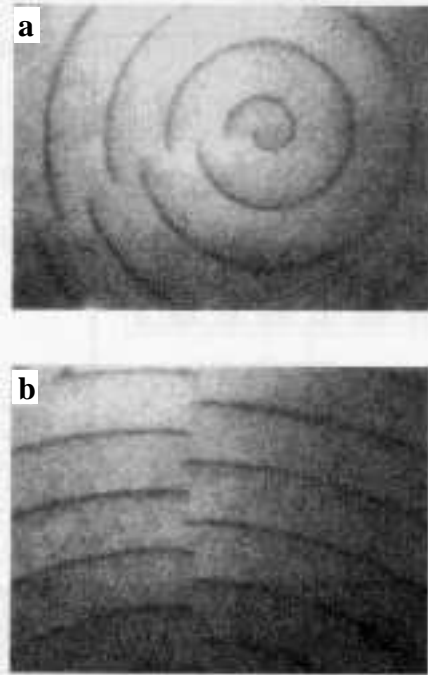


FIG. 6. Spiral wave with synchronization defect line on the surface of the ruthenium catalyzed BZ reagent. Panel (b) shows continuation of the defect line seen in panel (a). Reproduced with permission from Ref. [15].

One immediately recognizes a period-doubled spiral waveform with characteristic alternation of high and low maxima and clearly visible synchronization defect line like that shown in Fig. 4. The configuration in Fig. 6 is stable and was observed in the experiment for more than 30 min until the concentrations of consumable chemicals in the medium fell below some critical value and it was no longer possible to detect fluorescence of the wave.

Very recently, a set of controlled experiments on the BZ reaction under different conditions was carried out by Park and Lee [16] with the aim of observing synchronization defect lines and determining some of their properties. The wave patterns were seen in a continuously fed unstirred reactor composed of a 0.65 mm thick polyacrylamide gel membrane sandwiched between two well stirred reservoirs of reagents. Patterns can be controlled by varying the compositions and flow rates of the reservoirs and can be observed for arbitrarily long times since

the reagents are continuously refreshed.

For certain composition values and flow rates they observed a complex pattern of spiral waves which, upon analysis, was shown to comprise period-2 and period-3 spirals along with domains with more complicated dynamics separating these spiral wave regions. Both the period-2 and period-3 spirals exhibited synchronization defect lines, in some cases more than one defect line. For example, the period-2 spirals had either one or three defect lines. The defect lines themselves had spiral geometry and slowly rotated with some angular velocity, similar to those observed in simulations on the Willamowski-Rössler reaction-diffusion system. [11]

We shall comment further on additional features seen in these experiments below since the observations of Park and Lee also provide experimental evidence for line-defect turbulence which is discussed in Sec. VI.

## B. Structure of synchronization defect lines

The structure of the period-2 spiral wave in Fig. 4 may be analyzed by introducing a polar coordinate frame  $(r, \theta)$  with origin at the core of the wave. To quantitatively describe the sharp changes in the local dynamics across the synchronization defect line, one needs to find a local “order parameter” able to distinguish between the various loops of the local dynamics. In the present case, it is convenient to take advantage of the nature of the time series  $c_z(\mathbf{r}, t)$  and define the local order parameter as  $\delta_1 c_z(\mathbf{r})$ , the difference between two successive maxima of  $c_z(\mathbf{r}, t)$ . Figure 7, upper panel, shows  $\delta_1 c_z(\theta)$  for three values of  $C$  as function of the polar angle  $\theta$  along the arc segment that crosses the  $\Omega$  curve. To a very good approximation, the numerical data show that  $\delta_1 c_z(r, \theta, C)$  varies like

$$\delta c_z(r, \theta, C) \simeq A(r) \sqrt{C - C_1^*} \tanh[\kappa r (\theta - \theta_\Omega) (C - C_1^*)], \quad (4)$$

where  $\theta_\Omega$  is the angular position of the  $\Omega$  curve and  $\kappa$  is a numerical factor. The overall amplitude radial profile  $A(r)$  is similar to that of a spiral wave in a simple oscillatory medium. The  $\sqrt{C - C_1^*}$  factor reflects the supercritical nature of the period-doubling bifurcation. The  $\Omega$  curve is thus an exponentially localized object whose width remains approximately constant with  $r$  and varies like  $1/(C - C_1^*)$ . As  $C$  approaches  $C_1^*$  from above, the width increases until it becomes comparable to  $2\pi$  and the  $\Omega$  curve ceases to be a well-defined object.

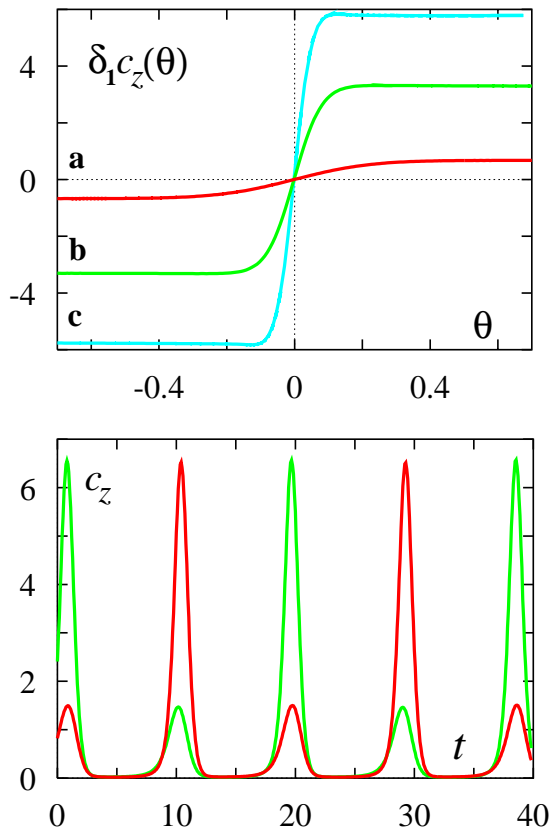


FIG. 7. The change of the local dynamics across the  $\Omega$  curve. Upper panel shows  $\delta_1 c_z(\theta)$  along the arc at radius  $r_0 = 130$  indicated in Fig. 4 for three values of  $C$ : (a)  $C = 3.04$ , (b)  $C = 3.10$ , (c)  $C = 3.84$ . Bottom: two  $c_z(t)$  concentration time series calculated at points  $\mathbf{r}_{1,3} = (r_0 = 130, \theta_\Omega \pm 0.05)$  on opposite sides of the  $\Omega$  curve.

To demonstrate that the  $\Omega$  curve corresponds to a one-dimensional synchronization defect, two  $c_z(t)$  concentration time series calculated at nearby spatial points on either side of the  $\Omega$  curve are shown in the bottom panel of Fig. 7. The two oscillations are shifted relative to each other by half a period. The nature of this shift can be understood from the observation of the local orbit loop exchange which occurs on the scale of the  $\Omega$  curve width. Figure 8 shows local orbits calculated at five different points on the arc shown in Fig. 4 with  $r_0 = 130$  and monotonically increasing  $\theta$ .

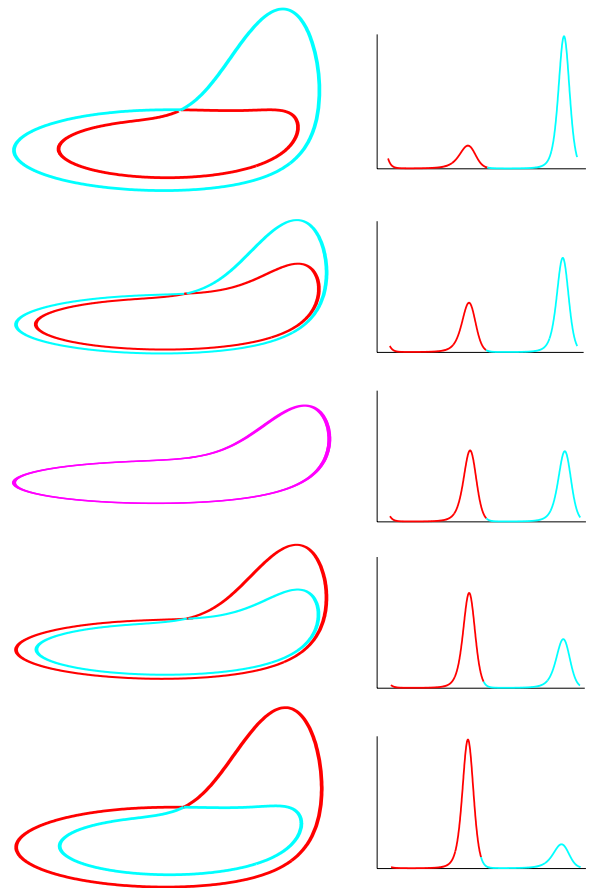


FIG. 8. Loop exchange in local orbits as the  $\Omega$  curve is crossed. Right column displays the  $c_z(\theta, t)$  time series corresponding to the orbits in  $(c_x, c_y, c_z)$  phase space shown in the left column. To highlight the exchange the first half of an oscillation period for each orbit is colored differently from the second half.

As one traverses the arc, the larger, outer loop of the local orbit constantly shrinks while the smaller, inner loop grows. At  $\theta = \theta_\Omega$ , both loops merge and then pass each other exchanging their positions in phase space. (Compare top and bottom panels of Fig. 8.) The behavior of the  $\delta_1 c_z(\theta)$  order parameter along the arc provides only limited information on the loop exchange. As one sees from Fig. 8, at the exchange point  $\theta = \theta_\Omega$  not only are the  $c_z$  maximum values of two loops equal ( $\delta_1 c_z(\theta_\Omega) = 0$ ), but the entire loops coincide in phase space and the local oscillation is effectively period-1.

Similar transformations of local orbits are observed in the excitable system shown in Fig. 5 as the defect lines are crossed. Figure 9 shows the  $v(\mathbf{r}, t)$  time series at four neighboring locations in the medium along a path intersecting one of the defect lines. Panel (a) is a plot of the normal  $\mathbf{1}^2$  dynamics seen on one side of the defect line. Every third minimum is lower than the two preceding minima and corresponds to the larger relaxation loop in the phase space plot.

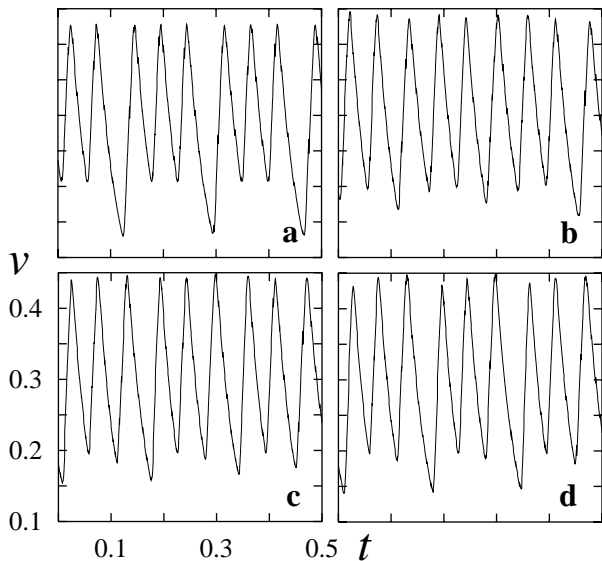


FIG. 9. Change in character of local dynamics across one of the defect lines seen in Fig.5. See text for details.

As one approaches the defect line, the large-amplitude loop shrinks while both small-amplitude loops grow (Fig.9(b)). Then, one small-amplitude loop begins to grow faster than the other and at some point becomes larger than the still shrinking large-amplitude loop (Fig.9(c)). This loop exchange process continues until the new large loop attains a size equal to that of a large-amplitude loop and the other two loops shrink to the size of the small-amplitude loop. The net result of this transformation is that the local time series on opposite sides of defect line appear to be shifted in time relative to each other by one third of the full period.

### III. PHASE DESCRIPTION OF SYNCHRONIZATION DEFECTS

The phenomena described in the previous section appear in systems with diverse reaction kinetics where complex oscillatory or excitable dynamics arises through completely different mechanisms. Nevertheless the structures of the spiral waves in these systems are similar, indicating the existence of a general organizing principle independent of the particular reaction mechanism. We now explain why defect lines are created to reconcile the rotation period of the spiral wave and the complex period of the local dynamics. The arguments presented here apply to a general complex-periodic system and are based on the observed local and global dynamics of the medium and not on the details of the of local reaction mechanism. Therefore, the discussion applies to oscillatory as well as driven and autonomous excitable systems with spiral waves.

To approach this problem one needs to consider how local complex-periodic or chaotic dynamics is synchronized

by diffusion into a global coherent pattern in the form of a spiral wave. The notion of phase plays a key role. In the period-1 regime the phase is an explicit, single-valued function of the concentrations  $\phi = \phi(\mathbf{c})$  and uniquely parameterizes a local orbit. After the first period-doubling this parameterization is no longer unique since the orbit does not close on itself when  $\phi$  changes by  $2\pi$ . The definition of phase for complex-periodic and chaotic oscillations is a difficult problem [17] and several possible definitions for the phase in such systems have been proposed. [18] For all such extended definitions the phase is no longer an observable since it cannot be calculated as a function of the instantaneous concentrations. In this section we generalize the definition of phase and show that although the absolute value of phase remains an arbitrary quantity, the phase difference between two oscillations of the same periodicity can be defined in a meaningful and robust way.

#### A. Phase of complex-periodic oscillations

Consider the orbit of a complex-periodic oscillation in a three-dimensional concentration phase space. We assume that the phase  $\phi(t)$  of an arbitrary period- $n$  oscillation is a scalar function of time which increases by  $2\pi n$  for each full period of the oscillation,  $T_n$ . In many cases  $\phi$  can be defined in terms of an angle variable  $\varphi$  in a suitably chosen coordinate frame. The phase variable  $\phi \in [0, 2\pi n)$  then takes the form

$$\phi = \varphi + 2\pi m, \quad (5)$$

where  $m$  is an integer with values from 0 to  $n - 1$ . For an  $n$ -periodic orbit,  $n$  of its points lie in a semiplane  $\varphi = \varphi_0$  for any  $\varphi_0 \in [0, 2\pi)$  (cf. Fig. 10) and the value of  $m$  serves to distinguish points with identical  $\varphi$ . While  $\varphi$  is a single-valued function of the original dynamical variables, the phase  $\phi$  of a complex-periodic oscillation is not an observable since a knowledge of the entire orbit is required in order to calculate  $m$ . At a period-doubling bifurcation, the parameterization given by the phase variable  $\phi$  changes discontinuously as  $m$  takes on twice as many possible values. This feature of the definition does not result in artificial discontinuities of any physical quantity since only the non-observable part  $2\pi m$  undergoes a jump. Figure 10 illustrates the definition of phase  $\phi$  for a period-2 orbit. Before the trajectory closes on itself the radius-vector executes two full turns and the orbit is naturally parameterized by  $\phi \in [0, 4\pi)$ .

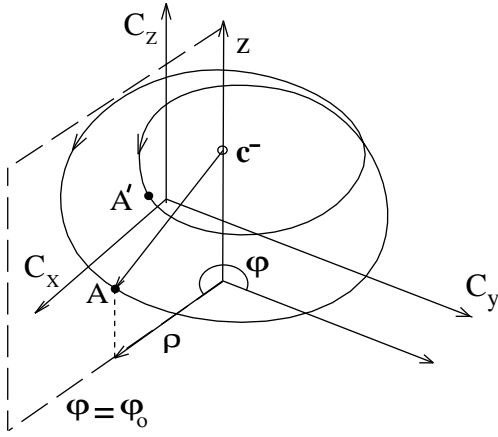


FIG. 10. Period-2 orbit in the  $(c_x, c_y, c_z)$  concentration phase space. Two points  $A$  and  $A'$  lying in the semiplane  $\varphi = \varphi_0$  have phases  $\phi_A = \varphi_0$  and  $\phi_{A'} = \varphi_0 + 2\pi$  which differ by  $2\pi$ .

The phase  $\phi(t)$  of an  $n$ -periodic oscillation may be written as

$$\phi(t) = \phi(0) + \int_0^t \omega(\tau) d\tau, \quad (6)$$

where

$$\omega(\tau) = A_0 + \sum_{k=1}^{\infty} \left( A_k \cos \frac{2\pi k}{T_n} \tau + B_k \sin \frac{2\pi k}{T_n} \tau \right)$$

is a  $T_n$ -periodic function of time with average  $A_0 = 2\pi n/T_n$ . Performing the integration in (6) we can rewrite  $\phi(t)$  as

$$\begin{aligned} \phi(t) &= \phi(0) + A_0 t + C + \psi(t), \quad (7) \\ C &= \frac{T_n}{2\pi} \sum_{k=1}^{\infty} \frac{B_k}{k}, \end{aligned}$$

where  $\phi(0)$  and  $C$  are constants depending on the initial conditions and the definition of  $\omega(\tau)$ , and  $\psi(t)$  is a  $T_n$ -periodic function with zero average.

Consider two oscillations with the same period  $T_n$  described by the same orbit in phase space but shifted in time such that  $\phi(t) \neq \phi'(t)$ . Since  $A_0 = A'_0 = 2\pi n/T_n$ , for the phase difference  $\delta\phi(t) = \phi(t) - \phi'(t)$  we get

$$\delta\phi(t) = \phi(0) - \phi'(0) + \frac{T_n}{2\pi} \sum_{k=1}^{\infty} \frac{B_k - B'_k}{k} + \psi(t) - \psi'(t). \quad (8)$$

Averaging (8) over  $T_n$  gives

$$\begin{aligned} \overline{\delta\phi} &= \frac{1}{T_n} \int_0^{T_n} [\phi(t) - \phi'(t)] dt = \quad (9) \\ &= \phi(0) - \phi'(0) + \frac{T_n}{2\pi} \sum_{k=1}^{\infty} \frac{B_k - B'_k}{k}, \end{aligned}$$

because both integrals of  $\psi(t)$  and  $\psi'(t)$  vanish separately. Since both oscillations differ only by a time shift  $\delta t \in [0, T_n)$  it is obvious that  $\phi'(t) = \phi(t - \delta t)$  and thus

$$\phi'(t) = \phi(0) + A_0(t - \delta t) + C + \psi(t - \delta t).$$

Performing the average of  $\delta\phi(t)$  again and equating the result to (9) we finally obtain

$$\overline{\delta\phi} = \phi(0) - \phi'(0) + \frac{T_n}{2\pi} \sum_{k=1}^{\infty} \frac{B_k - B'_k}{k} = A_0 \delta t. \quad (10)$$

The quantity

$$\delta\Phi = A_0 \delta t = 2\pi n \delta t / T_n,$$

unlike  $\delta\phi(t)$ , is independent of time and corresponds to the time delay of one oscillation with respect to the other expressed in fractions of the full-period phase increment  $2\pi n$ . For harmonic oscillations of the form  $A \cos(\omega t + \delta\phi)$  with  $\omega = 2\pi/T$ ,  $\delta\Phi$  coincides with the well-known notion of phase  $\delta\phi$ . Note that  $\delta\Phi$  does not depend on the precise definition of the phase  $\phi(t)$  as long as it is assumed that  $\phi(t)$  changes by  $2\pi n$  in one full period of the oscillation. Moreover, in Eqs. (6–10) the phase  $\phi(t)$  is not assumed to be a monotonic function of time and  $\omega(t)$  can change its sign. We only require that  $\omega(t)$  has period  $T_n$  and average value  $2\pi n/T_n$ . This allows one to define  $\delta\Phi$  even in those cases where a  $(\varphi, \rho, z)$  frame cannot be chosen so that  $\varphi$  grows monotonically with time and  $\phi$  uniquely parameterizes the orbit. The quantity  $\delta\Phi$  also possesses the important property of additivity. Consider three oscillations described by the same orbit in phase space and same period  $T_n$  but nevertheless non-identical  $\phi_1(t) \neq \phi_2(t) \neq \phi_3(t)$ . From (10) one finds that the pairwise differences  $\delta_{12}\Phi, \delta_{23}\Phi, \delta_{13}\Phi$  satisfy the relationship

$$\delta_{13}\Phi = \delta_{12}\Phi + \delta_{23}\Phi. \quad (11)$$

From the above discussion it follows that one can use the time averaged quantity  $\delta\Phi$  as the phase difference for complex periodic oscillations and this definition of  $\delta\Phi$  will be used below.

## B. Phase description of the medium

In a spatially-distributed system the shape of the local orbit generally depends on  $\mathbf{r}$  and, therefore, two oscillations at points  $\mathbf{r}_1$  and  $\mathbf{r}_2$  cannot be matched by simple time translation of one oscillation by  $\delta t$ . Nevertheless it is possible to define  $\delta\Phi(\mathbf{r}_1, \mathbf{r}_2)$  if one assumes that the local oscillations in the medium have the same period  $T_n$  everywhere apart from, perhaps, some set of points with zero measure. Consider two points in the medium  $\mathbf{r}'$  and  $\mathbf{r}''$  and a path  $\gamma$  connecting them so that for all  $\mathbf{r} \in \gamma$  the local oscillations have period  $T_n$ . Let us partition the curve  $\gamma$  into short segments by a set of points

$\mathbf{r}_i \in \gamma$ ,  $i = 0, 1 \dots l$  such that  $\mathbf{r}_0 = \mathbf{r}'$ ,  $\mathbf{r}_l = \mathbf{r}''$ . The length of the segments can be chosen sufficiently small so that due to the continuity of the medium the local dynamics at the adjacent points  $\mathbf{r}_i$  and  $\mathbf{r}_{i+1}$  is described by the same orbit and the phase difference  $\delta\Phi(\mathbf{r}_i, \mathbf{r}_{i+1})$  is defined in the sense of the previous section. Then  $\delta\Phi(\mathbf{r}', \mathbf{r}'')$  can be defined as a sum of  $\delta\Phi(\mathbf{r}_i, \mathbf{r}_{i+1})$  along  $\gamma$ . Applying (10) and (11) one finds

$$\begin{aligned} \delta\Phi(\mathbf{r}', \mathbf{r}'') &= \sum_{i=0}^{l-1} \delta\Phi(\mathbf{r}_i, \mathbf{r}_{i+1}) = \\ &= \sum_{i=0}^{l-1} \left( \phi_0^{i+1} - \phi_0^i + \frac{T_n}{2\pi} \sum_{k=1}^{\infty} \frac{B_k^{i+1} - B_k^i}{k} \right) = \\ &= \phi_0^l - \phi_0^0 + \frac{T_n}{2\pi} \sum_{k=1}^{\infty} \frac{B_k^l - B_k^0}{k}. \end{aligned} \quad (12)$$

Defined as a sum of infinitesimal phase shifts  $A_0 \delta t(\mathbf{r}_i, \mathbf{r}_{i+1})$ , the quantity  $\delta\Phi(\mathbf{r}', \mathbf{r}'')$  can be formally equated to  $A_0 \delta t(\mathbf{r}', \mathbf{r}'')$  with  $\delta t(\mathbf{r}', \mathbf{r}'')$  being the time translation which one should apply to the oscillation at point  $\mathbf{r}'$ , together with the simultaneous deformation of the orbit, to make it correspond with oscillation at point  $\mathbf{r}''$ . From (12) it follows that  $\delta\Phi(\mathbf{r}'', \mathbf{r}')$  does not depend on the choice of  $\gamma$  and the partition by  $\mathbf{r}_i$  since the contributions of all intermediate points  $\mathbf{r}_i$  cancel. Taking the continuous limit in (12) gives the integral form of the definition

$$\delta\Phi(\mathbf{r}_1, \mathbf{r}_2) = \int_{\mathbf{r}_1}^{\mathbf{r}_2} \nabla \delta\Phi(\mathbf{r}) \cdot d\mathbf{l}, \quad (13)$$

where  $d\mathbf{l}$  is an infinitesimal tangent to  $\gamma$ . The independence of  $\delta\Phi(\mathbf{r}_1, \mathbf{r}_2)$  on the path of integration endows it with some of the properties of a potential. On the other hand, due to the periodic nature of the phase, a non-zero circulation of  $\delta\Phi$  along closed loops is allowed as long as it is equal to an integer multiple of the full-period increment  $2\pi n$ .

Consider the phase variable field  $\phi(\mathbf{r}, t)$  at a time  $t$  and a contour integral of the phase gradient  $\nabla\phi(\mathbf{r}, t)$  taken along a closed loop  $\Gamma$  which surrounds the core of the spiral wave. For an arbitrary point  $\mathbf{r}_0 \in \Gamma$ , this loop is just a path in the medium which starts at  $\mathbf{r}_0$ , described by the local  $n$ -periodic oscillation phase  $\phi(\mathbf{r}, t)$ , and returns to the same point with same oscillation phase  $\phi(\mathbf{r}, t)$ . Thus, the integral may take only values  $2\pi nk$  equal to multiples of the full-period phase increment. From (5) the phase field is given by

$$\phi(\mathbf{r}, t) = \varphi(\mathbf{r}, t) + 2\pi m(\mathbf{r}, t),$$

and we find

$$\oint \nabla\phi(\mathbf{r}, t) \cdot d\mathbf{l} = \oint \nabla\varphi(\mathbf{r}, t) \cdot d\mathbf{l} + 2\pi \oint \nabla m(\mathbf{r}, t) \cdot d\mathbf{l}. \quad (14)$$

For a one-armed spiral with topological charge  $n_t = \pm 1$ , at any given time  $t$ ,

$$\oint \nabla\varphi(\mathbf{r}, t) \cdot d\mathbf{l} = \pm 2\pi,$$

regardless of the periodicity of the local dynamics. This follows from the fact that, by definition of  $\varphi$ , the  $\varphi(\mathbf{r}, t)$  field of a one-armed spiral wave in a medium with any periodicity is equivalent to that of a one-armed spiral wave in period-1 medium. Given that the full-period phase increment is  $2\pi$  only in the case of period-1 dynamics with  $m(\mathbf{r}, t) \equiv 0$ , for period doubled dynamics the integration of  $\nabla m(\mathbf{r}, t)$  along  $\Gamma$  must yield a non-zero contribution to balance (14). Since  $m(\mathbf{r}, t)$  is an integer function, its value changes discontinuously with time and space so that  $\nabla m(\mathbf{r}, t)$  can be different from zero only at a finite number of points which should possess a special, non-generic type of local dynamics. Consider the period-2 medium described in Sec. II. There it was shown that all the medium points with such non-generic dynamics constitute a continuous curve  $\Omega$  connecting the core of the spiral wave and the boundary, so that any contour  $\Gamma$  encircling the core must intersect  $\Omega$  at least in one point. The local oscillations on opposite sides of the  $\Omega$  curve were found to be shifted by half a period, which for a period-2 oscillation is equal to a  $2\pi$  phase translation.

It can be shown explicitly that on the  $\Omega$  curve the phase  $\phi(\mathbf{r}, t)$  undergoes a jump by  $2\pi$ . If one monitors the local dynamics while traversing the medium along the arc segment ( $r = r_0, \theta \in [\theta_\Omega - \Delta\theta, \theta_\Omega + \Delta\theta]$ ) intersecting the  $\Omega$  curve (see Fig. 4) one finds a progression of period-2 orbits whose loops rapidly converge to each other in phase space. For all  $\theta < \theta_\Omega$  the two loops can be distinguished from each other and are parameterized by  $\phi \in [0, 4\pi)$ . At  $\theta = \theta_\Omega$  the loops coalesce and the parameterization is given by period-1 phase  $\phi \in [0, 2\pi)$ . At the point  $\theta = \theta_\Omega + \varepsilon$ ,  $\varepsilon \rightarrow +0$  the oscillation is again period-2 but the loops are exchanged. Maintaining continuity of the parameterization (e.g.,  $m = 0$  on the smaller loop and  $m = 1$  on the larger) one finds that  $\phi(\theta_\Omega - \varepsilon, t) = \phi(\theta_\Omega + \varepsilon, t) + 2\pi$  for small  $\varepsilon > 0$  and any  $t$ . Obviously, as  $\varepsilon \rightarrow 0$  the discontinuity in the concentrations can be avoided only if at  $\theta = \theta_\Omega$  both  $\phi$  and  $\phi + 2\pi$  parameterize the same point on the orbit. This implies a period-1 oscillation which is indeed found at  $\theta_\Omega$ .

A simple example of the spatial distribution of the oscillation phase is presented in Fig. 11 which schematically shows a period-2 medium with spiral wave and single  $\Omega$  curve. A circular contour  $\Gamma$  is parameterized by the angle  $\theta \in [0, 2\pi)$  and  $\delta\Phi(\theta_0, \theta)$  is plotted in the third dimension above the corresponding point  $\theta$  on the contour. As one follows  $\Gamma$  clockwise, the phase difference  $\delta\Phi(\theta_0, \theta)$  grows monotonically up to  $\theta = \theta_\Omega$  where it experiences sudden  $2\pi$  jump and then increases continuously until the full-period phase increment of  $4\pi$  is reached at the point of the departure  $\theta_0$ .

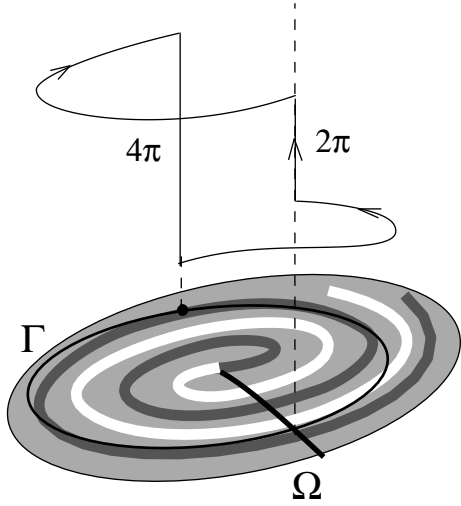


FIG. 11. Advance of the oscillation phase along contour  $\Gamma$  in the period-2 medium. The local angle variable field  $\varphi(\mathbf{r}, t_0)$  of a spiral wave is schematically shown by grey shades.

Similar considerations apply to the system with super-normal excitability shown in Fig. 5. For the medium with

period-3 local dynamics the continuity argument (14) requires that the total phase increment along  $\Gamma$  is equal to  $6\pi$ . Taking into consideration that the crossing of one of the defect lines leads to a  $2\pi$  phase shift, this requirement is easily satisfied by the presence of the two defect lines seen in Fig. 5. Indeed, the total phase increment  $\Delta_{\Gamma}\phi = 2\pi$  resulting from the integration of  $\nabla\phi(\mathbf{r}, t_0)$  along  $\Gamma$ , excluding its intersections with defect lines, plus the two  $2\pi$  phase jumps at the intersection points gives the expected  $6\pi$  phase increment.

#### IV. SYNCHRONIZATION DEFECTS IN MEDIA WITH HIGHER PERIODICITY: PERIOD-4

The continuity argument presented in the previous section requires that the sum of the phase jumps associated with defect lines emanating from the spiral wave core equal the full-period phase increment of the local dynamics  $2\pi nk$  minus  $2\pi$  from the spiral wave itself. It does not specify which types of synchronization defect are possible in a medium with given periodicity or how they are organized.

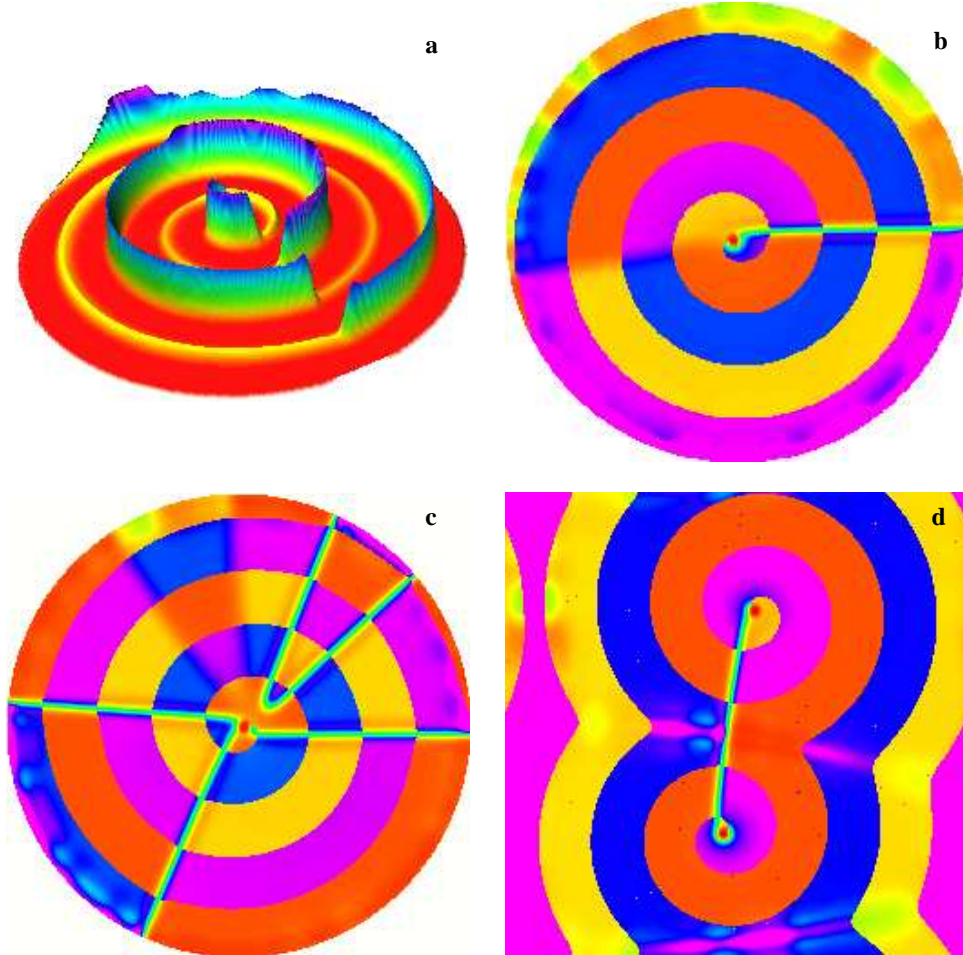


FIG. 12. Synchronization defect lines in Rössler media with period-4 dynamics for  $C = 4.30$ : (a) – instantaneous  $c_z(\mathbf{r})$  concentration profile of a single spiral wave is shown both by elevation and color; (b) – synchronization defects in the medium shown in panel (a) are visualized using the procedure described in text; (c) – result of evolution from different initial conditions; (d) – minimal defect configuration with one  $\Omega_1$  line connecting spiral wave cores in a domain with periodic boundary conditions.

As  $n$  increases one expects the diversity of defects will grow since the total phase shift associated with defect lines increases. Experimental investigation of systems with high periodicity is difficult since the size of the parameter domain where period- $n$  dynamics is found often rapidly decreases with  $n$ . Given the high dimensionality of parameter spaces for real systems, this makes experimental observation of complex-periodic regimes with large  $n$  difficult. Moreover, noise, which is inevitably present in every experiment, obliterates the fine features of the dynamics with large  $n$  and effectively sets an upper limit on the observable periodicity. Nevertheless, higher periodic dynamics has been observed in chemical systems; for instance, the period-3 spirals in the Park and Lee experiment [16] and the early stages of the period doubling cascade in the well-stirred BZ reaction [19]. Therefore, it is important to consider dynamics with  $n > 2$ . As an introduction to this topic in this section we consider systems with period-4 dynamics arising from period doubling of the period-2 dynamics described earlier. In the next section we generalize these considerations to period doubled dynamics of any order and to systems with general period- $n$  dynamics.

As the parameter  $C$  is increased, the Rössler medium supporting a spiral wave undergoes second period-doubling at  $C_2^* = 4.075$ . The transition to period-4 dynamics results in the doubling of the spiral wavelength, while the wave preserves its one-armed geometry. Therefore, the instantaneous concentration profile of the spiral wave normal to its front exhibits four different maxima corresponding to four different loops of the local orbit. It is convenient to number these loops according to their position in phase space starting from innermost loop. Then, up to cyclic permutations, the wave maxima follow each other in the order  $4 \rightarrow 1 \rightarrow 3 \rightarrow 2$ . This is the order in which the loops are visited during one full period of the dynamics. In period-2 media the identification of

synchronization defect lines based on the instantaneous concentration profiles was possible due to the significant difference between the loops of the local orbit in concentration phase space. For  $n \geq 4$ , where such differences are more subtle, different techniques are needed to identify synchronization defects. To achieve this the  $c_z$  concentration maxima were computed at every point in the medium during one spiral rotation and color-coded. Figure 12 shows the result of this procedure for two disk-shaped media and a system with two spiral waves in a domain with periodic boundary conditions at  $C = 4.30$ . Defect lines can be seen as radial discontinuities in color. (The spiral-shaped discontinuity is the inevitable artifact of the method: points lying on opposite sides of this line are collected at times separated by one quarter of the full oscillation period.) After one spiral rotation the colored bands exchange according to the permutation  $\begin{pmatrix} 1234 \\ 3421 \end{pmatrix}$  defined by the order of loop succession. Naturally, it takes four spiral rotations for the pattern to return to itself. The homogeneity of colors away from the boundary seen in Fig. 12(b) demonstrates that the local dynamics strictly follows a period-4 pattern whose characteristics are independent of location in the medium. Conversely, significant fluctuations of color near the boundary (disk-shaped media) and where the two spiral waves collide (periodic boundaries) show that the local dynamics is irregular in these regions. This shock line phenomenon is discussed in detail in Sec. VI.

Visual inspection of Fig. 12 shows the existence of two types of defect line which we denote  $\Omega_1$  and  $\Omega_2$ . As in the case of the prototypical  $\Omega$  curve, a certain value of the phase shift, expressed in fractions of the full-period phase increment  $8\pi$ , is associated with crossings of the  $\Omega_1$  and  $\Omega_2$  curves. Figure 13 (upper panels) shows the local  $c_z(\mathbf{r}, t)$  time series calculated on opposite sides of the  $\Omega_1$  and  $\Omega_2$  curves.

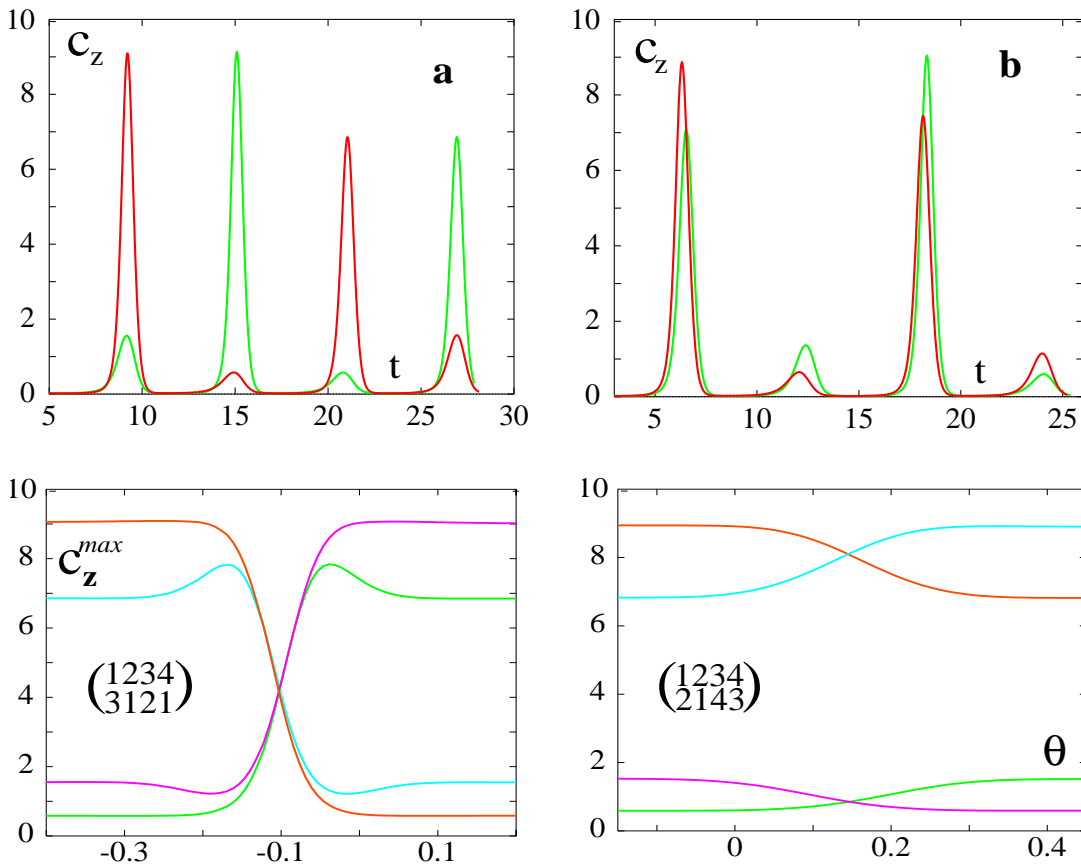


FIG. 13. Structure of synchronization defect lines in the period-4 regime: left column  $-\Omega_1$  defect, right column  $-\Omega_2$ . Upper row of panels shows local  $c_z(t)$  time series calculated on the opposite sides of corresponding defect lines. Lower row of panels displays corresponding loop exchanges (see text). Lines of the same color correspond to  $c_z(\theta)$  maxima calculated at the same time instant.

Similar to the  $\Omega$  curve, crossing of  $\Omega_2$  leads to a half-period shift which amounts to a  $4\pi$  phase translation. The specific nature of the half-period time shift is such that it is not possible to determine which oscillation is advanced, since a translation by  $T_4/2$  forward is equivalent to a shift by  $T_4/2$  backward. This is not the case for the crossing of the  $\Omega_1$  line where the oscillation acquires a quarter-period  $+2\pi$  or minus quarter-period phase shift  $-2\pi \equiv 6\pi$ , depending on the direction of crossing.

As in the period-2 medium, the phase discontinuity on the  $\Omega_1$  and  $\Omega_2$  curves results from loop exchanges. It is convenient to denote the loop exchanges by permutations which specify for every loop with number  $\ell$  of the oscillation pattern on one side of the defect, the loop with number  $m$  which is executed by the local dynamics on the other side of the defect at the same time instant. Thus, for the crossings of the  $\Omega_1$  curve in opposite directions, different loop exchange permutations are assigned:  $\begin{pmatrix} 1234 \\ 3421 \end{pmatrix}$  for the  $+2\pi$  shift and  $\begin{pmatrix} 1234 \\ 4312 \end{pmatrix}$  for  $-2\pi$ . A simple representation of the complex loop exchange process can be achieved by the following procedure. Consider an arc segment which intersects a line defect and is parameterized by the angle  $\theta$ . Calculation of the  $c_z$  concentration max-

ima during one full oscillation period  $T_4$  at every point on the segment gives four curves which intersect at those values of  $\theta$  where the corresponding loops exchange. The result of this procedure applied to both  $\Omega_1$  and  $\Omega_2$  curves is shown in Fig. 13 (lower panels). One sees that in the middle of the  $\Omega_2$  curve there exists a point at which the local orbit is period-2 and, thus, every two points with phases  $\phi$  and  $\phi + 4\pi$  become equivalent. The phase shift by  $2\pi$  on the  $\Omega_1$  curve formally takes place at the point with period-1 dynamics. This requires the intersection of all four curves in Fig. 13 at a single point which is structurally unstable. Therefore in the simulations one finds that the exchange  $\begin{pmatrix} 1234 \\ 3421 \end{pmatrix}$  is distributed over few neighboring mesh nodes where the dynamics appears to be represented by “noisy” (finite thickness) period-1 orbits.

The asymptotic configuration of defect lines in period-4 media depends both on boundary and initial conditions. If the medium shown in Fig. 4 is taken as the initial condition and the parameter  $C$  is increased past the transition to the period-4 dynamics, the  $\Omega$  curve undergoes a transformation into the  $\Omega_1$  curve. Although such a configuration with a single  $\Omega_1$  curve connecting the wave core and the boundary is the minimal line defect configu-

ration which satisfies continuity condition (14), it is certainly not the only possible one. If the initial conditions are taken sufficiently far from the asymptotic state, in the course of evolution the medium can develop a number of defect lines of both types which either connect the spiral wave core to the boundary or form loops with both ends on the boundary (see Fig. 12(c)). Once formed, these configurations freeze due to the pinning of the free ends of the  $\Omega$  curves to the boundary. In simulations on domains with periodic boundary conditions, all spontaneously formed  $\Omega$  curves take the form of closed loops and lines joining the wave cores. In the absence of boundaries these metastable configurations anneal to the minimal configuration where all closed loops are eliminated and every pair of oppositely charged defects is connected by a common  $\Omega_1$  curve.

### V. CLASSIFICATION OF SYNCHRONIZATION DEFECT LINES

In the previous sections we have shown that the phase singularities associated with line defects are related to the exchange of loops in the local orbits. This fact suggests that there is a relation between the types and properties of defect lines that exist in complex-periodic media and the topological organization of local orbits. In this section we show how to enumerate the possible types of synchronization defect and determine their properties for a period- $n$  medium. For  $2^n$ -periodic oscillations which constitute a period-doubling cascade this question can be answered in full, while for the general case we give an algorithm for its solution.

One can represent the loop exchanges pertaining to a particular type of defect line symbolically by a permutation which, for loop  $m_i$ ,  $i = 1, \dots, n$ , of a period- $n$  orbit specifies another loop  $m_j$ ,  $j = 1, \dots, n$ ,  $j \neq i$  into which it transforms under the exchange. The exchange permutations contain information on the value and sign of the associated phase shift. To extract this information one needs to include the state of the local oscillation into the symbolic description. Since the phase jump on the  $\Omega$  curves is always an integer multiple of  $2\pi$ , to characterize the jump one needs only a coarse-grained description with  $2\pi$  being the minimum detectable quantum of the phase change. At  $t = t_0$  let the phase point of the period- $n$  orbit be somewhere on the  $m_1$ -th loop, [20] at  $t = t_0 + T_n/n$  on the  $m_2$ -th loop, and so on (where  $m_l \in [1, n]$ ,  $l \in [1, n]$ ,  $m \neq l$ ) until at  $t = t_0 + T_n$  the phase point returns to the  $m_1$ -th loop and the pattern  $(m_1, m_2, \dots, m_n)$  repeats. The symbolic string  $s = (m_1, \dots, m_n)$  constructed in this way captures the most significant gross features of the oscillation pattern it describes. In this representation the oscillation shifted by  $2\pi$  forward relative to  $s$  is given by the string  $(m_2, \dots, m_n, m_1)$  while the oscillation shifted by  $2\pi$  backward reads  $(m_n, m_1, \dots, m_{n-1})$ . Obviously, any phase translation by  $\pm 2\pi k$  is represented by one of the  $n$

cyclic permutations of the symbolic string  $s$ . To find how the crossing of particular line defect affects the phase of the local oscillation one needs to act with the corresponding exchange permutation on a trial symbolic string and compare the result to the initial state. Consider as an example the  $\Omega_2$  curve described by the exchange permutation  $\begin{pmatrix} 1234 \\ 2143 \end{pmatrix}$ . Acting with it on the trial state (4132) one finds

$$\begin{pmatrix} 1234 \\ 2143 \end{pmatrix} (4132) = (3241),$$

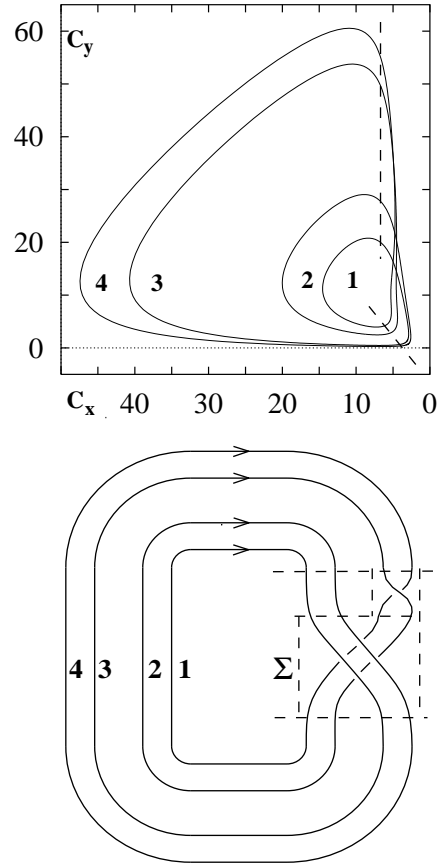


FIG. 14. Projection of the period-4 orbit of the Willamowski-Rössler system on the  $(c_x, c_y)$  plane (top) and the corresponding closed braid  $\overline{B}_4$  (bottom).

which corresponds to  $4\pi$  phase shift of the initial state. This result does not depend on the choice of the trial state. Action of the exchange permutation on any of the four different period-4 strings results in another string translated by  $4\pi$  relative to the initial string. In the general case of period- $n$  dynamics, the exchange permutations correspond to operators which map the set of all possible symbolic strings onto itself. Below we will show that these operators form a group.

To classify all synchronization line defects existing in the period- $n$  medium and find the associated phase shift values, one needs to identify all possible types of loop

exchange allowed by the topology of the orbit and select those that correspond to nontrivial phase translations. To approach this problem one needs a means to characterize a period- $n$  orbit topologically. Consider a period- $n$  orbit,  $P_n$ , consisting of  $n$  loops in the concentration phase space  $(c_x, c_y, c_z)$ . Using the cylindrical coordinate system introduced earlier, we may project  $P_n$  on the  $(\rho, \phi)$  plane preserving its original orientation and 3D character by explicitly indicating whether self-intersections correspond to over or under crossings. This procedure maps  $P_n$  onto a closed braid [21]  $\overline{B}_n$ . Figure 14 illustrates the construction of the braid representation for the  $P_4$  orbit. The direction of the flow is indicated by the arrows and the loops are numbered according to the convention introduced in Sec. IV. It is convenient to subdivide the closed braid  $\overline{B}_n$  into the open braid  $B_n$  (separated by dashed lines in Fig. 14) and its closure where threads run essentially parallel to each other.

A general open braid [22]  $b_n$  is a topological object which consists of  $n$  oriented threads forming a tangle as they run from one end to the other. Each crossing of the threads  $i$  and  $i + 1$  is assigned an elementary braid

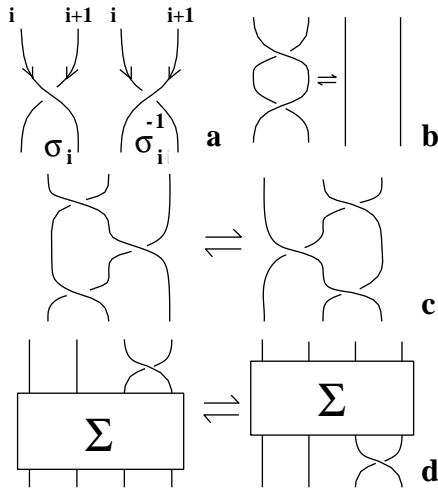


FIG. 15. Conventional designations and basic braid moves: (a) definition of elementary braids  $\sigma_i$  and  $\sigma_i^{-1}$ ; (b) type 2 Reidemeister move; (c) type 3 Reidemeister move, and (d) first Markov move ( $\Sigma$  represents arbitrary braid).

$\sigma_i$  if thread  $i$  overcrosses thread  $i + 1$  and  $\sigma_i^{-1}$  if it undercrosses thread  $i + 1$  (see Fig. 15(a)). Any braid  $b_n$  is described by a braid word that lists all elementary braids  $\sigma_i$  as they are encountered from the top of  $b_n$  to its bottom (convention for direction). For example,  $B_4$  as shown in Fig. 14 is described by the braid word  $\sigma_3\sigma_2\sigma_1\sigma_3\sigma_2$ . If  $\sigma_i$  and  $\sigma_j$  are on the threads with non-overlapping numbers their order can be exchanged and the corresponding commutation relation reads

$$\sigma_i\sigma_j = \sigma_j\sigma_i, \quad |i - j| \geq 2.$$

Without violation of its topology  $b_n$  can be transformed

into braids described by different braid words according to the set of elementary moves [21].

- The type 2 Reidemeister move,

$$\sigma_i\sigma_i^{-1} = \sigma_i^{-1}\sigma_i = \hat{\mathbf{1}},$$

allows one to simplify braid words by stating that the two threads that appear to cross but, in fact, are not entangled can be deformed into unit braid consisting of parallel threads (see Fig. 15(b)).

- The type 3 Reidemeister move,

$$\sigma_i\sigma_{i+1}\sigma_i = \sigma_{i+1}\sigma_i\sigma_{i+1},$$

illustrated in Fig. 15(c) completes the set of elementary operations.

By closing a braid  $b_n \rightarrow \overline{b}_n$  one makes it an object of more general topological nature. Indeed, any link or knot can be represented as a closed braid. For closed braids two additional moves can be applied to change the braid word.

- Type 1 Reidemeister (or second Markov) move which does not preserve the number of loops is not allowed in our studies of periodic orbits whose periodicity given by the number of loops is an essential invariant feature.
- The first Markov move

$$\sigma_i\Sigma = \Sigma\sigma_i,$$

where  $\Sigma$  belongs to the set of open braids, is shown in Fig. 15(d) and allows fragments of the braid to propagate around the closure of  $\overline{b}_n$  so that they can change their position from the top of  $\overline{b}_n$  to the bottom and vice-versa.

#### A. Loop exchanges as braid moves: period-2 example

We now examine possible loop exchanges for the period- $2^n$  period-doubled orbits and show how these exchanges influence the corresponding patterns of oscillation (unless specifically stated, the index  $n$  designates the power of 2 and not the full periodicity  $2^n$ ). A period-2 orbit is represented by the simplest nontrivial braid  $\overline{B}_2 = \overline{\sigma}_1$  shown in Fig. 16. Consider the first Markov move  $\mathcal{M}_1^{(1)}$  which propagates the elementary braid  $\sigma_1$  by  $2\pi$  around the braid  $\overline{B}_2$  in a direction opposite to the flow.

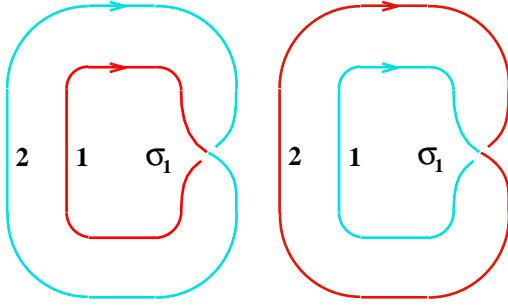


FIG. 16. Propagation of  $\sigma_1$  around the  $\overline{B_2}$  braid results in the exchange of loops.

The superscript in parentheses denotes the power  $n$  while the subscript numbers the moves consecutively. Although the braid  $\overline{B_2}$  remains unchanged as a result of this move, one finds that the two loops have interchanged their positions. To indicate this the loops of  $\overline{B_2}$  are drawn in different line styles in Fig. 16. The left panel shows  $\overline{B_2}$  before the application of  $\mathcal{M}_1^{(1)}$  and the right panel after. The interchange of loops induced by  $\mathcal{M}_1^{(1)}$  can be described by the exchange operator  $\mathcal{A}_1^{(1)}$  represented by the permutation  $\begin{pmatrix} 12 \\ 21 \end{pmatrix}$ . In the framework of the coarse-grained symbolic description, a period-2 oscillation has only two non-identical states  $s_1 = (12)$  and  $s_2 = (21)$ . Action of  $\mathcal{A}_1^{(1)}$  on one of them gives the other and vice-versa

$$\mathcal{A}_1^{(1)} s_1 = \begin{pmatrix} 12 \\ 21 \end{pmatrix} (12) = (21) = s_2,$$

$$\mathcal{A}_1^{(1)} s_2 = \begin{pmatrix} 12 \\ 21 \end{pmatrix} (21) = (12) = s_1.$$

One sees that the action of  $\mathcal{A}_1^{(1)}$  is equivalent to translation of the oscillation pattern by half a period, which for the period-2 oscillation amounts to a  $2\pi$  phase shift. To undo the result of the application of  $\mathcal{M}_1^{(1)}$  one needs to perform the reverse move  $(\mathcal{M}_1^{(1)})^{-1}$  which propagates  $\sigma_1$  along the flow or repeat  $\mathcal{M}_1^{(1)}$  once more. Thus, in terms of the exchange permutations the inverse operator  $(\mathcal{A}_1^{(1)})^{-1}$  induced by  $(\mathcal{M}_1^{(1)})^{-1}$  is equivalent to  $\mathcal{A}_1^{(1)}$  and produces the same action on the symbolic strings. From the properties discussed above, the operator  $\mathcal{A}_1^{(1)}$ , which symbolically represents the transformation of the period-2 oscillation on the  $\Omega$  curve, generates a group

$$(\mathcal{A}_1^{(1)})^{-1} = \mathcal{A}_1^{(1)}, (\mathcal{A}_1^{(1)})^{-2} = (\mathcal{A}_1^{(1)})^2 = \hat{1}. \quad (15)$$

In this way the exchange operators and algebraic relations between them can be established for period-doubled orbits with higher  $n$ . A detailed discussion of the period-4 case is presented in the Appendix where we consider all allowed braid moves and associated exchange operators for the  $P_4$  orbit and show that the  $\Omega_1$  and  $\Omega_2$  lines discussed above are the only types of synchronization defect in a period-4 medium.

## B. General case

A generalization of the formalism for the period-2 and period-4 (see Appendix) cases to a period- $2^n$  orbit  $P_{2^n}$  may be derived from the observation of the structural organization of the corresponding closed braids  $\overline{B_{2^n}}$ . This does not require the enumeration of all possible braid moves whose number quickly grows with  $n$ . Indeed, to find all types of synchronization defect allowed in the period- $2^n$  medium one only needs to identify those moves that result in nontrivial translations of the oscillation pattern.

A braid  $\overline{B_{2^{n+1}}}$  can be obtained from  $\overline{B_{2^n}}$  by doubling each thread of  $\overline{B_{2^n}}$  and adding a single crossing on the top of the braid to preserve the simple connectivity of the construction. The braid  $\overline{B_{2^n}}$  arising as a result of  $n$  successive iterations of this

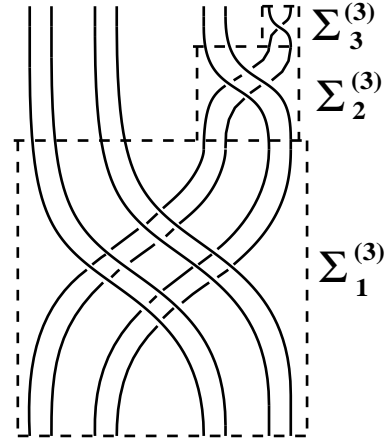


FIG. 17. Braid  $B_8$  constructed for the period-8 orbit

procedure can be subdivided into  $n$  non-overlapping structurally similar blocks of braids  $\Sigma_m^{(n)}$ ,  $m = \overline{1, n}$ . This principle of structural organization is illustrated in Fig. 17 for  $B_8$  and its three braid blocks are shown in a series of boxes with decreasing size. The analysis shows that these blocks can be moved as individual entities along  $\overline{B_{2^n}}$  without interference, and produce an exchange of the loops along which they move. The essential parts of these transformations can be represented by a set  $\mathcal{M}_m^{(n)}$  of  $2\pi$  moves of structural blocks  $\Sigma_m^{(n)}$  so that  $\mathcal{M}_1^{(n)}$  corresponds to the largest block and results in an exchange involving all the  $2^n$  loops,  $\mathcal{M}_2^{(n)}$  corresponds to movement of next-smaller braid block and results in the exchange of  $2^{n-1}$  loops, and so on. The transformations of the time trajectories resulting from exchanges of loops can be again described by the action of permutation operators  $\mathcal{A}_m^{(n)}$  on symbolic strings  $s_j$ . The fact that the crossing blocks move independently implies that operators  $\mathcal{A}_m^{(n)}$  commute. The geometry of  $\overline{B_{2^n}}$  also defines the

basic algebraic property of the  $\mathcal{A}_m^{(n)}$ . The generalization of (15) gives

$$(\mathcal{A}_i^{(n)})^{2^i} = \hat{\mathbf{1}}, \quad \mathcal{A}_i^{(n)} \circ \mathcal{A}_j^{(n)} = \mathcal{A}_j^{(n)} \circ \mathcal{A}_i^{(n)}, \quad (16)$$

where  $i, j \in [1, n]$ . Those compositions of exchange operators which are induced by moves returning  $\overline{B}_{2^n}$  to itself (see Appendix for examples of moves changing the configuration of the braid) yield translation operators  $\mathcal{T}_{\pm 2\pi k}$  where  $k \in [1, 2^{n-1}]$ . To identify these operators one does not have to enumerate all possible compositions, whose number grows exponentially with  $n$ . Indeed, since translation by  $2\pi k$  is equivalent to  $k$  times a translation by  $2\pi$  and, thus  $\mathcal{T}_{2\pi k} = (\mathcal{T}_{2\pi})^k$ , it is only necessary to find the generator  $\mathcal{T}_{+2\pi}$  of the subgroup of translators  $\mathcal{T}_{2\pi k}$ . For the period- $2^n$  orbits this problem can be solved exactly for any  $n$ .

As mentioned earlier, the configuration of  $B_{2^n}$  determines the succession rule which states the order in which the loops are visited during one period of oscillation. For example, consider again  $B_4$  (see Fig. 14). Following the direction of the flow one can find the order in which loops succeed each other after they pass through the tangle of  $B_4$ . Writing the result as a permutation  $\begin{pmatrix} 1234 \\ 3421 \end{pmatrix}$  one sees that it corresponds to the permutation representation of  $\mathcal{T}_{+2\pi}$ , since phase translation by  $2\pi$  is essentially equivalent to the advance of the oscillation by  $T_{2^n}/2^n$  prescribed by the succession rule. This result obviously holds for any  $n$ . Thus, if the entire braid  $B_{2^n}$  is propagated around its closure by  $2\pi$ , the result is formally equivalent to the composition of all elementary moves  $\mathcal{M}_m^{(n)}$  applied one by one and the net loop exchange is given by the succession rule. Therefore, the sought-for operator  $\mathcal{T}_{+2\pi}$  is induced by the composition  $\mathcal{M}_1^{(n)} \circ \mathcal{M}_2^{(n)} \dots \circ \mathcal{M}_n^{(n)}$  and any translation operator  $\mathcal{T}_{2\pi k}$  is given by

$$\mathcal{T}_{2\pi k} = \left( \prod_{m=1}^n \mathcal{A}_m^{(n)} \right)^k, \quad (17)$$

where  $k = [-2^{n-1}, 2^{n-1}]$ . Indeed, from the results of the previous section for  $n = 2$  it follows that

$$\mathcal{T}_{4\pi} = (\mathcal{A}_2^{(2)})^2 = (\mathcal{A}_1^{(2)} \circ \mathcal{A}_2^{(2)})^2 = (\mathcal{T}_{2\pi})^2.$$

In principle, every nontrivial translation operator  $\mathcal{T}_{2\pi k}$  corresponds to a different type of synchronization line defect and in the period- $2^n$  oscillatory medium one should be able to find  $2^{n-1}$  different types of  $\Omega$  curve. Thus for period-8 system the following types of line defects with corresponding exchange operators are possible:

$$\begin{aligned} \Omega_1^{(3)} (\pm 2\pi) & \quad \mathcal{A}_1^{(3)} \circ \mathcal{A}_2^{(3)} \circ \mathcal{A}_3^{(3)}, \\ \Omega_2^{(3)} (\pm 4\pi) & \quad (\mathcal{A}_2^{(3)})^2 \circ (\mathcal{A}_3^{(3)})^2, \\ \Omega_3^{(3)} (\pm 6\pi) & \quad \mathcal{A}_1^{(3)} \circ (\mathcal{A}_2^{(3)})^3 \circ (\mathcal{A}_3^{(3)})^3, \\ \Omega_4^{(3)} (8\pi) & \quad (\mathcal{A}_3^{(3)})^4. \end{aligned}$$

A half-period translation of period-8 oscillation which occurs at the crossing of the  $\Omega_4^{(3)}$  curve is induced by the

propagation of the simple crossing  $\Sigma_3^{(3)}$  four times around the closure of  $\overline{B}_8$ . By analogy with the cases  $n = 1, 2$  one can predict that in the middle of the  $\Omega_4^{(3)}$  curve there exists a point where the oscillation is period-4. The analysis of the exchange operator  $(\mathcal{A}_2^{(3)})^2 \circ (\mathcal{A}_3^{(3)})^2$  leads to the conclusion that on  $\Omega_2^{(3)}$  one should find a point with effective period-2 dynamics. The operator  $\mathcal{A}_1^{(3)}$  which stands for the exchange of the period-2 bands of period-8 orbit appears in the above list twice: for the  $\Omega_1^{(3)}$  and  $\Omega_3^{(3)}$  curves. Therefore, period-1 dynamics should be observed on both lines. Since it is unlikely to observe the exchange of all eight loops in the same medium point due to its structural instability, the actually observed dynamics should be given by thick, “noisy” period-1 orbits. In the next section, show that pure period- $2^n$  local dynamics with  $n \geq 3$  is not observed in media with spiral waves. Nevertheless, period-8 local dynamics can be observed in media without spiral waves (see below). Indeed, all four possible  $\Omega$  curve types with predicted characteristic features have been found in such media.

For the more general case of period- $n$  local dynamics where  $n$  is not a power of 2 resulting from a period-doubling cascade, the following algorithm can be employed. First, the local orbit  $P_n$  should be mapped onto a closed braid  $\overline{B}_n$ . Then through the analysis of the topology of  $\overline{B}_n$  the blocks of elementary braids which can be moved independently should be identified. Their  $2\pi$  propagation around the closure of  $\overline{B}_n$  will give a set of essential braid moves with corresponding exchange operators. Those compositions of the essential moves which lead to the identity transformation of  $\overline{B}_n$  should result in some nontrivial phase translations. These phase shifts, in turn, should correspond to possible types of  $\Omega$  curve.

## VI. LINE DEFECT TURBULENCE

Thus far we have considered the description and analysis of line defects in systems with period-2 and period-4 dynamics in the period doubling cascade. Now, again using the Rössler reaction-diffusion equation as our model system, we examine its behavior as the parameter  $C$  is increased causing the system enter chaotic regimes. We describe the nature of these regimes for spatial configurations with and without spiral waves and show how their structure is related to the dynamics of synchronization line defects.

In the computations presented below, we consider both systems with a single spiral in medium with no-flux boundary conditions, as well as systems with periodic boundary conditions supporting several spiral waves. For the Rössler reaction-diffusion system, configurations with many spiral waves form spatially blocked structures. The blocked structures form irregular cellular patterns with cells centered on the spiral wave cores. The polygonal

boundaries of the cells are delimited by shock lines where the spiral waves from neighboring cells collide. Figure 12 (d) shows a simple example of such a blocked cellular pattern with two spiral waves.

### A. Transition to chaos in the presence of spiral waves

Figure 18 shows the bifurcation diagram for the Rössler medium supporting a solitary spiral wave, measured at a point  $\mathbf{r}$  in the “bulk” region, i.e. away from both the spiral core and boundary regions. To show the first two period-doubling bifurcations, the local order parameter  $\delta_m c_z(\mathbf{r})$  was redefined as the maximum difference between  $c_z$  concentration maxima calculated at point  $\mathbf{r}$  in one full period  $T_4$  of the period-4 oscillation. In the period-2 regime this quantity coincides with  $\delta_1 c_z(\mathbf{r})$  introduced earlier, while in the period-4 domain it gives the difference between the fourth (the highest) and first (the lowest)  $c_z$  maxima. The dependence of  $\delta_m c_z(C)$  for the Rössler ordinary differential equations is also shown for comparison in Fig. 18. One sees that the period-doubling bifurcations in the bulk of the medium are shifted to the right along the parameter  $C$  axis with respect to bifurcations observed in the ODE. Indeed, the local dynamics in the medium controlled by a spiral wave resembles the dynamics of the ODE at some  $C'$  which is always less than the value of  $C$  in the PDE. The value of  $\Delta C = C - C'$  depends on the wavelength  $\lambda$  of the wave pattern in the medium and vanishes as  $\lambda \rightarrow \infty$ . If more than one spiral wave is present, similar considerations apply to the shock lines between spiral domains where incoming waves collide. The normal wave pattern is broken on these shock lines and the local dynamics is also shifted to higher  $C$  values compared to the dynamics in the bulk. In fact, at  $C$  values corresponding to the period-4 dynamics in the bulk, the dynamics on the shock lines already exhibits chaos which manifests itself in the fluctuations of color seen in Fig. 12. Chaos first occurs on the shock lines, for  $C$  values approximately equal to those for the onset of chaos in the Rössler ODE, in agreement with the fact that the phase gradient is zero along the shock lines.

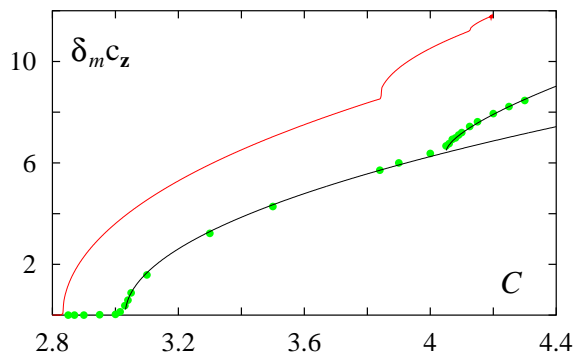


FIG. 18. Domain of period doubling oscillations in the Rössler medium supporting a spiral wave. The upper dashed curve is for the Rössler ordinary differential equation.

The entire period-doubling cascade to chaos is *not* observed when the bifurcation parameter  $C$  is increased further. One finds instead a complex scenario which involves turbulent stages characterized by spontaneous formation, erratic motion and proliferation of synchronization defect lines. To characterize line-defect turbulence quantitatively one needs a means to both visualize the dynamics of the  $\Omega$  lines and measure their density. The color-coding technique introduced earlier allows only visualization. To solve this problem scalar fields were defined [23] in the following way: during four consecutive rotations of the spiral wave the values of the  $c_z(\mathbf{r})$  concentration maxima  $A_i(\mathbf{r})$ ,  $i = 1, 4$  were collected at every point in the medium and sorted so that  $A_1(\mathbf{r}) \leq A_2(\mathbf{r}) \leq A_3(\mathbf{r}) \leq A_4(\mathbf{r})$ . The scalar fields are defined as  $\xi_1(\mathbf{r}) = A_4(\mathbf{r}) - A_1(\mathbf{r})$  and  $\xi_2(\mathbf{r}) = A_4(\mathbf{r}) - A_3(\mathbf{r})$ . By construction,  $\xi_1(\mathbf{r})$  and  $\xi_2(\mathbf{r})$  take on fixed, non-zero values at points in the medium with period-4 dynamics and vanish at points where the loop exchanges occur. Indeed,  $\xi_1(\mathbf{r})$  decreases to zero on the  $\Omega_1$  curves while  $\xi_2(\mathbf{r})$  vanishes on both the  $\Omega_1$  and  $\Omega_2$  curves. The  $\xi_1(\mathbf{r})$  and  $\xi_2(\mathbf{r})$  fields allow one both to determine the lengths of the  $\Omega$  curves and to visualize them. Figure 19, panel (c), shows the  $\xi_2(\mathbf{r})$  field at  $C = 4.3$  for a medium with periodic boundary conditions supporting a spiral pair. The corresponding  $\varphi(\mathbf{r}, t_0)$  and  $c_z(\mathbf{r}, t_0)$  fields are shown in panels (a) and (b), respectively. The cores of spiral waves, seen as black disks, are connected by a common  $\Omega_1$  curve which appears as a wide, nearly straight black line. At this value of  $C$  the dynamics in the bulk of the medium (spiral cores,  $\Omega_1$  curve, and shock lines excluded) is given by a period-4 pattern (see Fig. 20(a)) and single  $\Omega_1$  curve connecting the cores constitutes the minimal configuration which satisfies the continuity condition (14). The shock lines, where the spiral waves collide, are seen in panels (c) and (d) as one vertical and two horizontal strips where the grey shades are inhomogeneous. This inhomogeneity in the  $\xi_2(\mathbf{r})$  field indicates that the local dynamics on the shock lines is different from that in the bulk. Indeed, the calculations show that the local dynamics on the shock lines at  $C = 4.3$  is given by two-banded chaos (see Fig. 20(b)). The chaotic dynamics on the shock lines gives rise to spatially coherent fluctuations of  $A_i(\mathbf{r})$  fields seen in Fig. 19(c) as darkly shaded “breathing spots”. Sufficiently large fluctuations (like that indicated by the arrow in the figure) may result in the creation of “bubbles” – domains delineated by circular  $\Omega_2$  curves (cf. Fig. 19(d)). For  $C \leq C_{\Omega_2} = 4.306$ , the bubbles are formed with a size smaller than a certain critical value and collapse shortly after birth. As  $C$  increases beyond  $C_{\Omega_2}$ , the bubble nuclei begin to proliferate, forming large domains whose growth is controlled by collisions with spiral cores or other domains (see next subsection for details about the dynamics of  $\Omega$  lines).

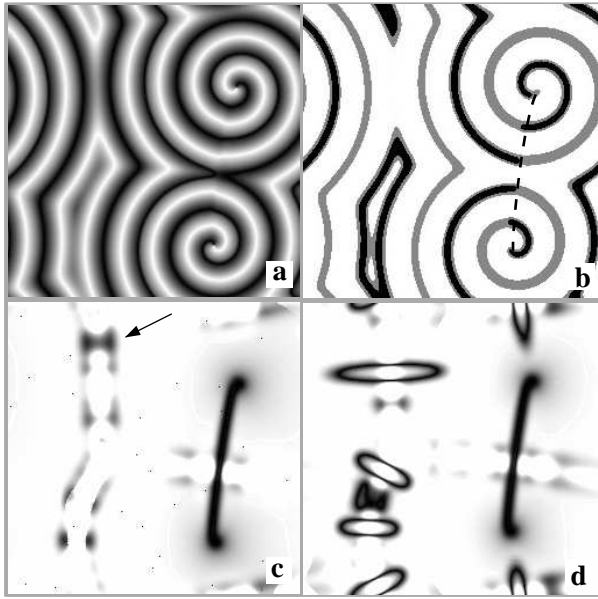


FIG. 19. Representation of defect lines by the  $\xi_2(\mathbf{r})$  field for the medium with two spiral waves at  $C = 4.30$  (c) and  $C = 4.32$  (d). Panels (a) and (b) show, respectively, the  $\varphi(\mathbf{r}, t_0)$  and  $c_z(\mathbf{r}, t_0)$  fields calculated for the medium in panel (c).

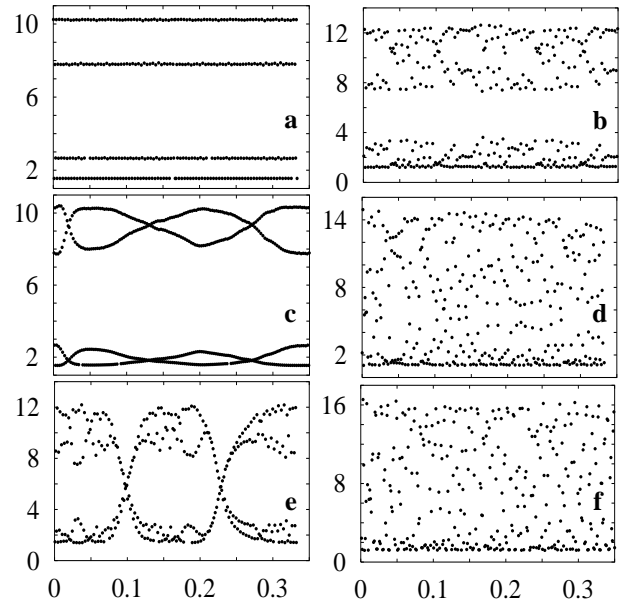


FIG. 20. Time series of the  $c_z$  concentration maxima: a,b)  $C = 4.30$ , c,d)  $C = 4.42$  and e,f)  $C = 4.7$ . Left panels show the local dynamics at a point in the bulk, while the right panels show the dynamics on the shock lines. Time is in units of thousands of spiral revolutions. In panels (c) and (e), respectively, the crossing of the  $c_z$  maxima reflect the passages of an  $\Omega_2$  or  $\Omega_1$  line through the observation point in the medium.

The transition to line-defect turbulence changes the character of the local dynamics observed in the bulk of the medium. As the  $\Omega_2$  lines propagate through the medium the associated loop exchanges result in an effective band-merging in the orbits of local trajectories so that they take the form of two-banded chaotic trajectories (cf. Fig. 20(c)). As  $C$  increases past  $C \approx 4.5$  the local dynamics fails to exhibit a period-4 pattern in the intervals separating line defect passages and shows thick four-banded orbits whose bands grow in width with increasing  $C$ . The width of chaotic bands varies from point to point and while in some locations one observes their merging, in others there might be a distinct gap between them. The local dynamics on the shock lines also progresses towards less-structured chaos. At  $C = 4.42$  (cf. Fig. 20(d)) it already exhibits one-banded chaos.

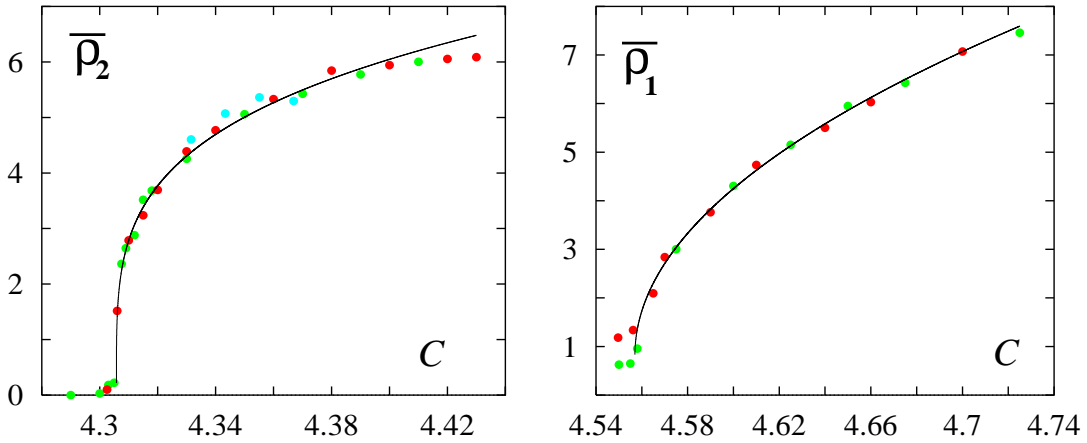


FIG. 21. Transition to  $\Omega_2$ - (left) and  $\Omega_1$ -line (right) turbulence. Green – system with two spirals shown in Fig. 19; red – system of the same size with four spirals; blue – system with two spirals but twice the linear dimension,  $L = 512$ .

As the parameter  $C$  approaches the second critical value  $C_{\Omega_1} \approx 4.557$  the shock lines begin to spontaneously nucleate bubbles of  $\Omega_1$  lines. At  $C > C_{\Omega_1}$  the newly-born domains delineated by  $\Omega_1$  lines begin to proliferate and fill the medium with a perpetually changing turbulent pattern. The defect line density can be used as an order parameter to characterize transitions to turbulence quantitatively. From the  $\xi_i(\mathbf{r})$ , ( $i = 1, 2$ ), fields the lengths  $\ell_i$  of the  $\Omega_i$  lines may be computed. The  $\Omega_i$  line density is then  $\rho_i(t) = \ell_i(t)/L$  where  $L$  is the linear dimension of the square array. Although the instantaneous values of  $\rho_i(t)$  fluctuate considerably, the balance between defect line growth and destruction results in a statistically stationary average density  $\bar{\rho}_i$  of  $\Omega_i$  lines. The time-averaged  $\Omega_i$  line densities  $\bar{\rho}_i$  as a function of  $C$  are plotted in Fig. 21. In all simulations the average intensity of noise on the shock lines was estimated from the calculations at  $C < C_{\Omega_i}$  and subtracted. Likewise, for construction of the diagram in Fig. 21(a) the contribution of the stationary  $\Omega_1$  line (see Fig. 19) was estimated and subtracted. The behavior of both averaged densities beyond the corresponding critical points shows a power law dependence,

$$\bar{\rho}_i(C) \sim (C - C_{\Omega_i})^{\alpha_i}, \quad (18)$$

with parameters ( $C_{\Omega_2} = 4.306$ ,  $\alpha_2 = 0.25 \pm 0.01$ ) and ( $C_{\Omega_1} = 4.557$ ,  $\alpha_1 = 0.49 \pm 0.02$ ) respectively. Such behavior indicates that both transitions to turbulence can be considered as non-equilibrium phase transitions [23].

The bands of the local orbits continue to grow in width and merge at  $C \approx 4.7$ . Globally this transition can be identified as spontaneous nucleation of  $\Omega_2$  bubbles homogeneously in the medium. These chaotic  $\Omega_2$  lines are loci of medium points where two chaotic bands of the local orbit shrink and a thick period-2 orbit is formed. With increase in  $C$  the width of these lines decreases and their motion in the medium becomes totally erratic. For  $C > 4.8$  the  $\Omega_2$  lines cease to exist as well-defined entities. Qualitatively the same scenario applies to the disappearance of  $\Omega_1$  lines. At  $C \approx 5.0$  one starts to find bubbles of  $\Omega_1$  lines not only in the shock zones but also in the bulk. This indicates the transition of the local dynamics to one-banded chaos homogeneously in the medium. For  $C \geq 5.1$  no defect lines can be identified and further increase in  $C$  does not result in any qualitative changes.

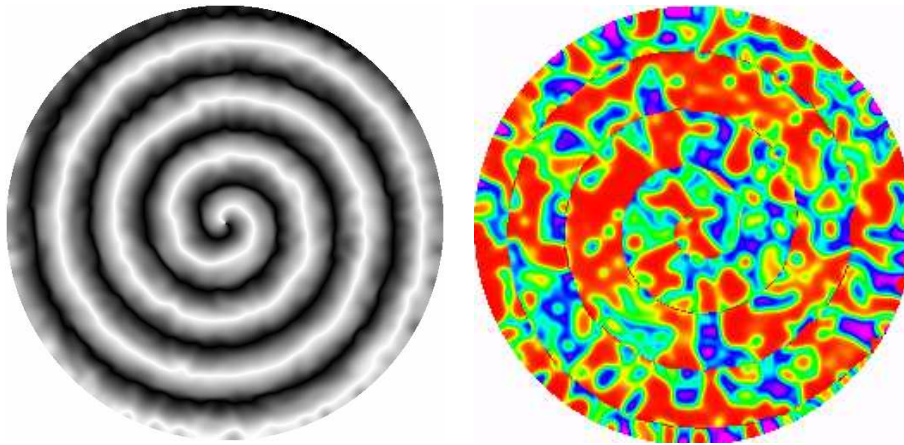


FIG. 22. Spiral wave in the deep chaotic regime at  $C = 5.9$ .

It is interesting to follow the fate of the spiral wave in chaotic regime. Even deep in the chaotic regime, where the local dynamics is represented by one-banded chaotic orbits, spatially coherent spiral dynamics can be still seen in the medium. [24–26,11] Figure 22, left panel, shows the local angle variable field  $\varphi(\mathbf{r}, t_0)$  for  $C = 5.9$ . A clearly visible image of the spiral wave with distorted equal-angle lines  $\varphi = \varphi_0$  signifies that chaotic oscillations remain synchronized [17] in the sense of period-1 phase  $\phi = \varphi$ . As the execution of any loop of the Rössler chaotic attractor takes approximately the same time and the motion occurs with nearly constant angular velocity  $d\varphi/dt \approx 2\pi/T_0$ , where  $T_0$  is the period of spiral revolution, the chaotic spreading of the local trajectories does not lead to break-up of  $\varphi$  synchronization. To demonstrate that the medium is indeed in a turbulent regime in which the amplitude of the local oscillations is disordered, the maximum  $c_z$  amplitude color-coding procedure described in Sec. IV was applied. One sees that the randomly varying  $c_z$  maxima constitute a turbulent pattern with very short correlation length.

In the experiments of Park and Lee [16] on the BZ reaction, configurations containing several period-2 and period-3 spiral waves separated by regions with complex dynamics were seen. Parameter domains were also inves-

tigated where the system exhibited turbulent dynamics. Within the turbulent regimes bubble-shaped  $\Omega$  lines and irregular  $\Omega$  line dynamics were observed, akin to the defect line turbulence phenomena described above.

### B. Dynamics of line defects

By following the dynamics of synchronization line defects in the turbulent regimes described above, one can make a number of observations important for understanding the factors governing growth, motion and destruction of  $\Omega$  lines. Figure 23 shows six consecutive frames of the  $\xi_2(\mathbf{r})$  field for a long interval of the evolution of  $\Omega_2$ -line turbulence at  $C = 4.38$ . When a supercritical nucleus of the  $\Omega_2$ -line domain is born on the shock line, it grows toward the spiral wave cores positioned on opposite sides of the shock line. As mentioned earlier, every spiral core is confined to a cell formed by the shock lines and, thus, within one such cell there exists only one center of attraction for the proliferating defect lines. Therefore, depending on whether the nucleus was formed on one shock line or the intersection of two shock lines, a domain may experience attraction to two or more spiral cores.

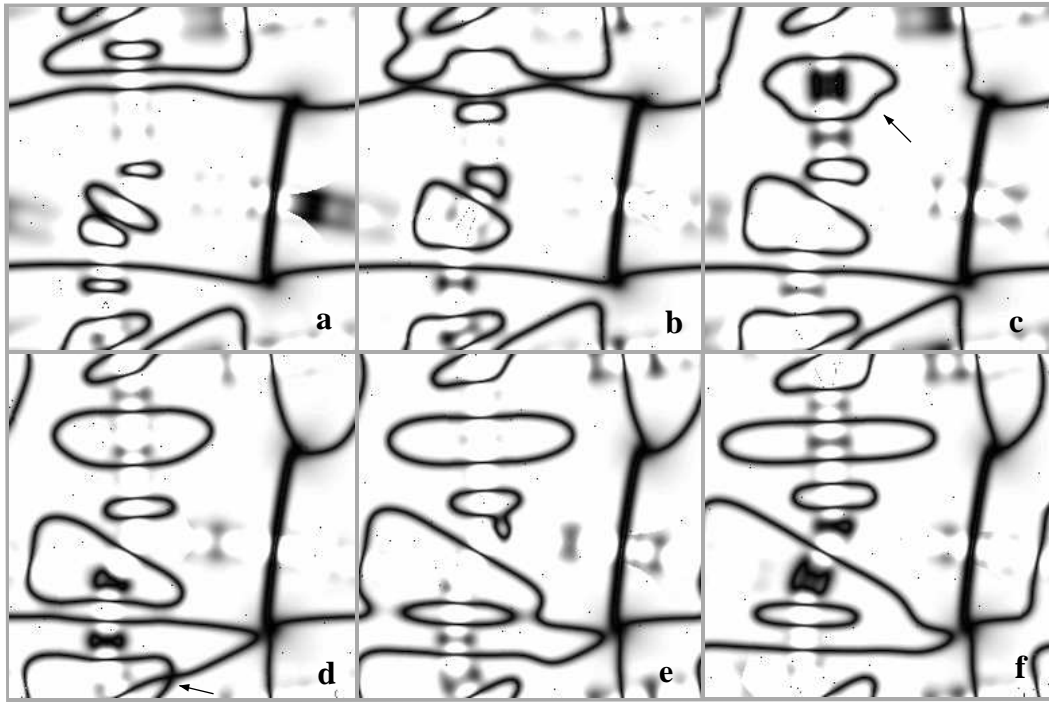


FIG. 23. The evolution of the medium with  $\Omega_2$ -line turbulence at  $C = 4.38$ . All panels are equally separated in time by 24 spiral revolutions and show the  $\xi_2(\mathbf{r})$  field coded by grey shades.

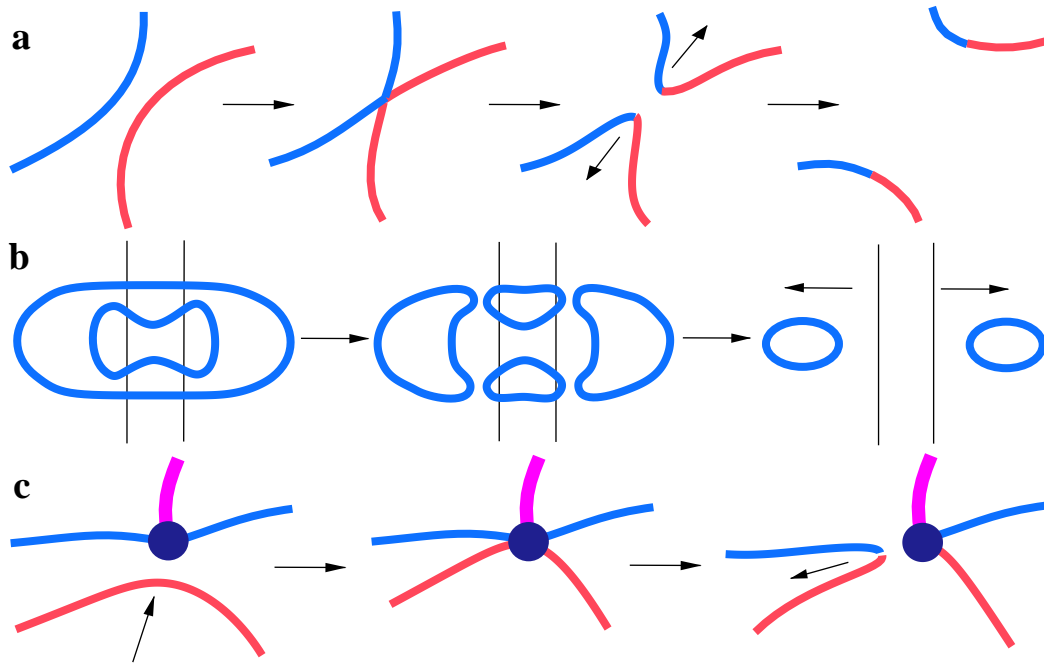


FIG. 24. Interaction of defect lines in the turbulent regime: a) reconnection of lines following contact, b) formation of bubbles disconnected from the shock line (indicated by two vertical solid lines), and c) reconnection of lines in the wave core (indicated by black disk). The arrows between the pictures show the sequence of events, while arrows on the pictures designate the direction of line defect motion.

The dynamics of  $\Omega_1$  lines in the regime of  $\Omega_1$ -line turbulence exhibits qualitatively the same features as  $\Omega_2$ -line dynamics. In the process of growth the domain is likely to collide with other expanding domains. The contact of  $\Omega_1$  and  $\Omega_2$  lines results in formation of one  $\Omega_1$  line. Where the lines coalesce, the phase shift across the  $\Omega_1$  line changes sign. Indeed, the composition of the loop exchanges corresponding to  $\Omega_1$  and  $\Omega_2$  lines results in a loop exchange which can be attributed to another  $\Omega_1$  line with opposite sign of the phase shift:  $\pm 2\pi + 4\pi = \mp 2\pi$ . The contact of two  $\Omega$  lines of the same type occurs according to the scenario which is sketched in Fig. 24(a). When two defect lines collide, they reconnect with change of their topology and net length. At the instant of collision an unstable state is formed in which the lines seem to intersect. The break-up of this state always occurs in the direction given by the bisectrices of the two acute angles. As a result the two initial defect lines break and two new lines are formed as shown in Fig. 24(a). Two bends with high curvature quickly straighten and the newly-formed lines depart from each other. Note, that this process leads to the reduction of the net length of  $\Omega$  lines. The major stages of the reconnection process are sketched in the bottom of panels (c)–(e) in Fig. 23. Panel (d) captures the intermediate crossover state (indicated by the arrow) which is difficult to detect due to its short life time. This elementary event which takes place locally when two lines come in contact can give rise to a variety of topologically different global configurations. For example, the contact of two domains may result in the formation of one large domain, or a large domain with a small one in its interior. The case where one domain forms inside the other is of particular interest (see Fig. 24(b)). In the process of their recombination two new domains disconnected from the shock line are formed. They quickly acquire a circular shape and begin to drift toward the wave cores simultaneously shrinking in size. In most cases the latter process predominates and the domains collapse before they can reach the cores.

Configurations with more than three  $\Omega$  lines emanating from the same spiral wave core appear to be unstable, at least for the Rössler medium we have studied. This is probably due to the fact that the size of the core is insufficient to accommodate more than three  $\Omega$  lines. Nevertheless, such configurations play the role of intermediate states in the process of line reconnection in the wave core. Figure 24(c) schematically shows the events that take place in the panels (c) and (d) of Fig. 23 in the neighborhood of the lower spiral core. When an  $\Omega_2$ -line loop reaches the core, an unstable configuration with one  $\Omega_1$  and four  $\Omega_2$  lines is created. As in the case of line contact, the unstable configuration breaks so that the two lines that form the sharpest angle produce a loop which disconnects from the core. Thus, reconnection of defect lines can also occur through the unstable line configuration at the spiral wave core.

From these observations it follows that the evolution of the size and shape of a domain is controlled by the

balance of two competing factors: propagation of defect lines along the phase gradient directed to the spiral wave cores which results in line growth, and the tendency of diffusion to eliminate curvature and reduce the length of defect lines. To investigate the interplay of these two factors a series of simulations was carried out on a rectangular system of size  $L_x \times L_y$  without spiral waves but with a shock line where the nucleation of  $\Omega$  lines may take place. Periodic boundary conditions were used in the  $x$  direction and constant concentrations corresponding to those in the spiral core were imposed at  $y = \pm L_y/2$ . To break the spatial translational symmetry of the system the fixed concentrations on the “core” boundaries were taken to have the form  $\mathbf{c}_0 + \zeta(r)$ , where  $\mathbf{c}_0$  is the concentration in the spiral core and  $\zeta(r)$  is a spatial white noise contribution. All other parameters were unchanged. In this geometry wave trains of plane waves emitted by the constant concentration boundaries

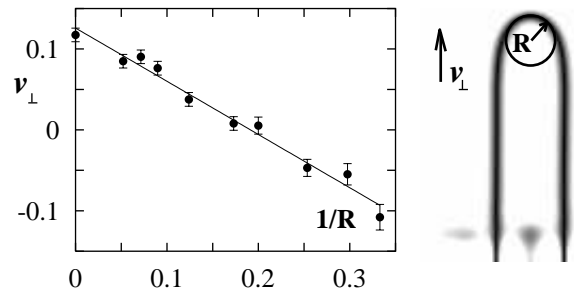


FIG. 25. Dependence of the domain propagation velocity,  $v_{\perp}$ , versus the curvature,  $1/R$ , of the tip for  $C = 4.30$ . A typical finger-shaped  $\Omega_2$  domain is shown in the right panel.

collide in the center of the system to form a shock line. The domains randomly formed on this shock line have very simple finger-like shapes, normal to the shock line, and consist of two straight segments with approximately semi-circular caps (see Fig. 25). The domain growth velocity  $v_{\perp}$  along  $y$  varies with the radius  $R$  of the arc of the growing tip as

$$v_{\perp} = v_p - \Delta/R \quad (19)$$

where the quantities  $v_p = 0.126$ , the velocity of a planar  $\Omega_2$  line along  $y$ , and  $\Delta = 0.658$  were calculated from the simulation data presented in Fig. 25. Since the width of small domains is approximately equal to  $2R$ , one can estimate the critical size that must be exceeded for domain expansion. From equation (19) the critical radius is  $R_c = 5.228$ , which is in good agreement with  $R_c$  directly measured from the observation of domains whose shape does not change with time. Also from (19) it follows that the velocity  $v_{\perp}$  is independent of the distance to the “core” boundary and is solely defined by the properties of the  $\Omega_2$ -line domain – the curvature  $1/R$  of its growing tip. The investigation of the  $\mathbf{c}(\mathbf{r}, t)$  field has shown the absence of concentration gradients along the  $y$  axis of the medium. On the basis of these results it was concluded

that the defect lines propagate along the local phase gradient  $\nabla\phi(\mathbf{r}, t)$ . In media with spiral waves, where the phase gradient is always directed to the wave core, this results in the motion seen as the propagation of defect lines to the wave core.

### C. Line defect turbulence in systems without spiral waves

It is interesting to contrast the phenomena described above for the Rössler system with spiral waves with those observed in the same medium without spiral waves. We studied this case by considering initial conditions where spatial inhomogeneities were sufficiently weak that spiral waves were not formed in the course of the dynamics. We observed that the onset of defect-line nucleation occurs at the same critical values  $C_{\Omega_i}$  as when spiral waves are present. In the absence of large-scale phase gradients, the entire medium behaves like the shock regions separating spiral wave cells, defect lines do not grow and the increase of  $\overline{p_i}(C)$  arises essentially from the enhanced nucleation rate. This leads to a different form of the onset of line turbulence characterized by different critical exponents ( $\beta_1^* = 1.22$ ,  $\beta_2^* = 0.53$ ). [23] These values are difficult to estimate because of fluctuations in the  $\xi_i$  fields not associated with fully developed  $\Omega$  lines. The fact that  $\beta_1^*$  and  $\beta_2^*$  are significantly different from  $\beta_1$  and  $\beta_2$  supports the conclusion that the character of the transitions is different in the spiral and spiral-free systems.

## VII. CONCLUSIONS

In this paper we presented a study of synchronization defect lines in two-dimensional complex-periodic and chaotic media. As for simple periodic media, stable spiral waves in such systems are one-armed and, therefore, characterized by a topological charge  $n_i = \pm 1$ . In one turn of such a spiral wave the local complex-periodic dynamics executes only a fraction of the full oscillation period and the concentration field does not return to its initial state. For example, in the period-2 medium it takes two rotations of the spiral for the concentration field to be restored. This conflict between the spiral rotation period and the period of the local oscillation is reconciled by the presence of a synchronization defect line connecting the wave core to the boundary or to another spiral wave core with opposite topological charge. The average of the continuity condition (14) over the full period  $T_n$  of the local  $n$ -periodic dynamics gives

$$\frac{1}{2\pi n} \oint \nabla\delta\Phi(\mathbf{r}) \cdot d\mathbf{l} = k, \quad (20)$$

a complex-periodic analog of (1) for a topological phase defect in a period-1 medium. As follows from (14), the full contour increment of  $2\pi nk$  consists of two different

parts. While  $2\pi$  is contributed by the integration of  $\nabla\delta\Phi(\mathbf{r})$  along  $\Gamma$ , the remaining  $2\pi(nk - 1)$  is gained by adding up phase jumps on the intersections with synchronization line defects. Thus,  $k$  in (20) does not characterize the topological phase defect whose charge remains  $\pm 1$ . Instead the value of  $k$  is defined by the particular configuration of the line defects emanating from the spiral wave core. Consider, for example, the period-4 case described in Sec. IV. Condition (20) selects possible configurations of  $\Omega$  curves emanating from the core. If the topological charge of the spiral wave core is positive ( $n_i = +1$ ) then the minimal configuration which satisfies (20) has one  $\Omega_1$  curve with phase shift  $-2\pi$  and corresponds to  $k = 0$ . The other configuration for  $k = 0$  is given by three  $\Omega_1$  curves with one positive and two negative signs ( $-2\pi + 2\pi - 2\pi$ ). For  $k = 1$  one also finds two admissible configurations. One is given by  $\Omega_1 (+2\pi)$  and  $\Omega_2 (4\pi)$  curves and the other consists of two  $\Omega_2$  curves and one  $\Omega_1$  curve with negative sign.

Synchronization defects also play an important role in the transition to chaos. In this transition, media supporting spiral waves exhibit line-defect turbulence characterized by proliferation, erratic motion and collision of defect lines. In this regime the dynamics of defects is controlled by two factors: growth along the phase gradient and the tendency of diffusion to reduce their length and curvature. The balance of these factors gives rise to a statistically stationary density of defect lines which varies with the parameters. A power-law form of this variation indicates that the transitions to line-defect turbulence can be considered as non-equilibrium phase transitions.

Synchronization defect lines have been observed in experiments on the BZ reaction by Yoneyama et al. [15] and Park and Lee [16]. Such defect lines should be observable more generally in spatially-distributed systems exhibiting various types of complex-periodic local dynamics. The organization of spiral waves in such systems is governed by general topological principles independent of the particular reaction mechanism. For example, it is possible that spiral waves give rise to pathological complex-periodic dynamics in systems with super-normal excitability, such as cardiac muscle. Indeed, mixed-mode electrical activity with alternating large and small amplitude maxima, so-called alternans, is typically observed as a symptom of tachycardia [27]. Therefore, self-organized spiral waves of electrical activity might be responsible for the emergence of this type of cardiac arrhythmia.

Finally, in three-dimensional media with complex local dynamics, we expect the scroll waves emitted by vortex filaments to be accompanied by synchronization defect surfaces transversally similar to the synchronization defect lines of two-dimensional media. Neither the three-dimensional organization of these surfaces nor their dynamics and interactions has been investigated.

## ACKNOWLEDGEMENTS

This research was supported in part by a grant from the Natural Sciences and Engineering Research Council of Canada.

## APPENDIX A: SYNCHRONIZATION DEFECTS AND BRAID MOVES; COMPLETE ANALYSIS FOR THE PERIOD-4 CASE

The set of transformations of a  $P_4$  orbit is much richer than that of a period-2 orbit but can be enumerated easily. Examination of  $\overline{B}_4$  (see Fig. 14) shows that the open braid  $B_4$  can be partitioned into two structural blocks:

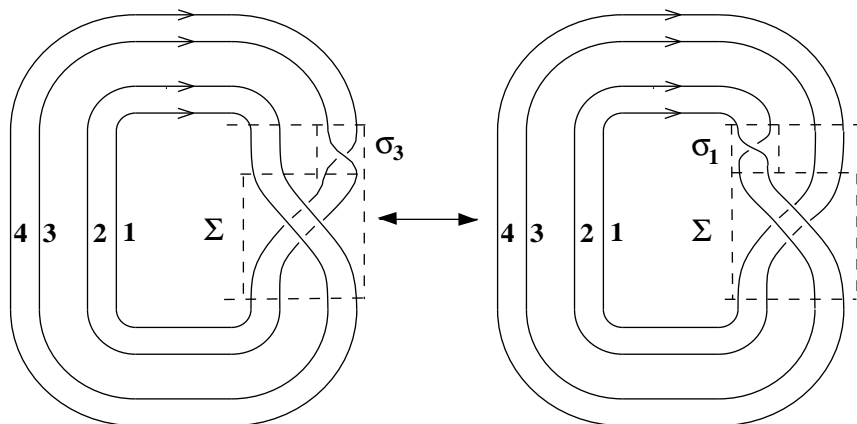


FIG. 26. Two alternative configurations of the  $\overline{B}_4$  braid:  $\Sigma_1 = \sigma_3 \Sigma$  (left) and  $\Sigma_2 = \sigma_1 \Sigma$  (right).

to two different succession rules defining the order in which the loops of  $P_4$  are visited during one full period of oscillation. Indeed, following the direction of the flow for  $\Sigma_2 = \sigma_1 \Sigma$  one finds an abnormal pattern  $4 \rightarrow 2 \rightarrow 3 \rightarrow 1$  which is not found in either spatially homogeneous or spatially distributed systems. As  $n$  grows, the number of different configurations for  $\overline{B}_{2^n}$  also increases although only one of them is actually exhibited by the dynamics. The exchange of loops produced by the application of  $\mathcal{M}_1^{(2)}$  can be characterized again by an exchange operator  $\mathcal{A}_1^{(2)}$  represented by a permutation  $\begin{pmatrix} 1234 \\ 3412 \end{pmatrix}$ . Acting with  $\mathcal{A}_1^{(2)}$  on any of the four period-4 symbolic strings, e.g.  $s_1 = (4132)$ , one finds a string which is not given by any cyclic permutation of  $s_1$  but instead belongs to permutations of the abnormal pattern  $s_1^* = (4231)$  induced by  $\Sigma_2$ . Therefore, an exchange of loops which is not induced by the braid move returning  $\overline{B}_{2^n}$  to its normal state does not correspond to any phase translation of the oscillation pattern. Due to the apparent similarity of action of  $\mathcal{M}_1^{(1)}$  and  $\mathcal{M}_1^{(2)}$  on the corresponding orbits,

the elementary crossing  $\sigma_3$  and  $\Sigma = \sigma_2 \sigma_1 \sigma_3 \sigma_2$ . These blocks can propagate through each other and, thus, can be moved independently. Let  $\mathcal{M}_1^{(2)}$  be a braid move which propagates  $\Sigma$  by  $2\pi$  in the direction opposite to the flow. Upon completion of this move  $\overline{B}_4$  is not returned to its initial state, instead  $\overline{B}_4$  is given by the braid  $\Sigma_2 = \sigma_1 \Sigma$  shown in Fig. 26 (right panel), where the elementary crossing occurs between loops 1 and 2. Note that  $\Sigma_1 = \sigma_3 \Sigma$  and  $\Sigma_2 = \sigma_1 \Sigma$  cannot be transformed into each other with braid moves affecting only the open braid part without resorting to the first Markov move which exchanges the loops. Therefore,  $\Sigma_1$  and  $\Sigma_2$  represent two principally different configurations of  $B_4$  which correspond

$\mathcal{A}_1^{(2)}$  inherits the algebraic properties of  $\mathcal{A}_1^{(1)}$ . Indeed,  $\mathcal{A}_1^{(2)}$  produces identity operator when applied twice and, thus, is equal to its inverse.

Finer rearrangement of the  $P_4$  loop structure is provided by the action of  $\mathcal{M}_2^{(2)}$  which moves the single crossing (enclosed in the smaller box in Fig. 26) by  $2\pi$  in the direction opposite to the flow. Again one finds that  $\mathcal{M}_2^{(2)}$  switches  $\overline{B}_4$  into its alternative configuration  $\Sigma_1 \leftrightarrow \Sigma_2$ . Depending on the initial state, the application of  $\mathcal{M}_2^{(2)}$  results in different loop exchanges. In the case of  $\Sigma_1 = \sigma_3 \Sigma$  action of  $\mathcal{M}_2^{(2)}$  leads to the exchange of loops 3 and 4 and results in the string transformation described by the exchange operator  $\mathcal{A}_2^{(2)}$  with symbolic representation  $\begin{pmatrix} 1234 \\ 1243 \end{pmatrix}$ . When it acts on  $\Sigma_2 = \sigma_1 \Sigma$  it exchanges loops 1 and 2 and the permutation representation of  $\mathcal{A}_2^{(2)}$  changes to  $\begin{pmatrix} 1234 \\ 2134 \end{pmatrix}$ . The inverse of  $\mathcal{M}_2^{(2)}$  moves the single crossing along the flow and produces opposite results; i.e., acting on  $\Sigma_1$  it leads to  $1 \leftrightarrow 2$  exchange and when applied to  $\Sigma_2$  it results in the exchange  $3 \leftrightarrow 4$ . Double application of  $\mathcal{M}_2^{(2)}$  or its inverse restores  $\overline{B}_4$  to its normal configuration and

the resulting loop exchange, given by  $(\mathcal{A}_2^{(2)})^2$  or  $(\mathcal{A}_2^{(2)})^{-2}$ , corresponds to a nontrivial phase translation. To demonstrate this let  $(\mathcal{A}_2^{(2)})^2$  act on the trial state  $s_3 = (3241)$ . Applying the rules one obtains

$$(\mathcal{A}_2^{(2)})^2 s_3 = \begin{pmatrix} 1234 \\ 2134 \end{pmatrix} \begin{pmatrix} 1234 \\ 1243 \end{pmatrix} (3241) = (4132) = s_1 = \mathcal{T}_{4\pi} s_3,$$

where operator  $\mathcal{T}_{4\pi}$  symbolically represents phase translation by  $4\pi$ . Thus, the simultaneous loop exchange (13)  $\leftrightarrow$  (24) corresponds to translation of the period-4 oscillation by half of a period. This implies as well that application of  $\mathcal{A}_2^{(2)}$  four times results in the identity string transformation  $(\mathcal{A}_2^{(2)})^4 = \mathcal{T}_{8\pi} = \hat{\mathbf{1}}$  and, therefore,  $(\mathcal{A}_2^{(2)})^{-1} = (\mathcal{A}_2^{(2)})^3$ .

Consider now compositions of braid moves  $\mathcal{M}_1^{(2)}$  and  $\mathcal{M}_2^{(2)}$ . Since both moves and their inverses alternate the braid configuration  $\Sigma_1 \leftrightarrow \Sigma_2$ , the application of the composition of any two of them returns braid  $\overline{B}_4$  into its initial state and, thus, the resulting string transformation is equivalent to some translation. As was stated earlier, the propagation of the two structural blocks of  $\overline{B}_4$  given by moves  $\mathcal{M}_1^{(2)}$  and  $\mathcal{M}_2^{(2)}$  is independent and, therefore, the corresponding exchange operators  $\mathcal{A}_1^{(2)}$  and  $\mathcal{A}_2^{(2)}$  commute

$$\begin{aligned} \mathcal{A}_1^{(2)} \circ \mathcal{A}_2^{(2)} &= \begin{pmatrix} 1234 \\ 1243 \end{pmatrix} \begin{pmatrix} 1234 \\ 3412 \end{pmatrix} = \mathcal{A}_2^{(2)} \circ \mathcal{A}_1^{(2)} = \\ &= \begin{pmatrix} 1234 \\ 3412 \end{pmatrix} \begin{pmatrix} 1234 \\ 2134 \end{pmatrix} = \begin{pmatrix} 1234 \\ 3421 \end{pmatrix} = \mathcal{T}_{+2\pi}, \\ \mathcal{A}_1^{(2)} \circ (\mathcal{A}_2^{(2)})^{-1} &= \begin{pmatrix} 1234 \\ 2134 \end{pmatrix} \begin{pmatrix} 1234 \\ 3412 \end{pmatrix} = (\mathcal{A}_2^{(2)})^{-1} \circ \mathcal{A}_1^{(2)} = \\ &= \begin{pmatrix} 1234 \\ 3412 \end{pmatrix} \begin{pmatrix} 1234 \\ 1243 \end{pmatrix} = \begin{pmatrix} 1234 \\ 4312 \end{pmatrix} = \mathcal{T}_{-2\pi}. \end{aligned}$$

Based on these considerations one may conclude that all possible loop exchanges for  $P_4$  constitute a group generated by the elements  $\mathcal{A}_1^{(2)}$  and  $\mathcal{A}_2^{(2)}$ . The relations between the elements of this group can be derived from the following rules:

$$(\mathcal{A}_1^{(2)})^2 = \hat{\mathbf{1}}, (\mathcal{A}_2^{(2)})^4 = \hat{\mathbf{1}}, \mathcal{A}_1^{(2)} \circ \mathcal{A}_2^{(2)} = \mathcal{A}_2^{(2)} \circ \mathcal{A}_1^{(2)}.$$

Those elements of this group which are induced by braid moves returning  $\overline{B}_4$  into its normal configuration correspond to nontrivial phase translations and, therefore, to different types of synchronization line defect. Thus,  $(\mathcal{A}_2^{(2)})^2$  describes the  $\Omega_2$  curve while  $\mathcal{A}_1^{(2)} \circ \mathcal{A}_2^{(2)}$  and its inverse represent the  $\Omega_1$  curve.

and Patterns, Kluwer Academic Publishers, Dordrecht, (1996).

- [2] A. Mikhailov, *Foundations of Synergetics I: Distributed Active Systems*, Springer, New York, (1994).
- [3] D. Walgraef, *Spatio-Temporal Pattern Formation*, Springer, New York, (1997).
- [4] N. D. Mermin, *Rev. Mod. Phys.*, **51**, 591 (1979).
- [5] P. S. Hagan, *SIAM J. Appl. Math.*, **42**, 762, (1982).
- [6] S. Scott, *Chemical Chaos*, Oxford University Press, New York, (1991).
- [7] D. Chialvo, D. Michaels, and J. Jalife, *Circ. Res.*, **66**, 525, (1990).
- [8] D. Barkley, *Physica D*, **49**, 61, (1991).
- [9] A. Giaquinta, S. Boccaletti, L. Tellini, and F. Arrecchi, *Chaos*, **4**, 557, (1994).
- [10] O. E. Rössler, *Z. Naturforsch.*, **31**, 1664, (1976).
- [11] A. Goryachev and R. Kapral, *Phys. Rev. E*, **54**, 5469, (1997).
- [12] A. Goryachev, H. Chaté, and R. Kapral, *Phys. Rev. Lett.*, **80**, 873, (1998).
- [13] K. D. Willamowski and O. Rössler, *Z. Naturforsch.*, **35**, 317 (1980).
- [14] A. Goryachev and R. Kapral, to appear in *Int. J. Bifurcation and Chaos*, (1999).
- [15] M. Yoneyama, A. Fujii, and S. Maeda, *J. Am. Chem. Soc.*, **117**, 8188, (1995).
- [16] J.-S. Park and K. J. Lee, to be published.
- [17] M. Rosenblum, A. Pikovsky, and J. Kurths, *Phys. Rev. Lett.*, **76**, 1804, (1996).
- [18] G. Osipov, A. Pikovsky, M. Rosenblum, and J. Kurths, *Phys. Rev. E*, **55**, 2357, (1997).
- [19] J. C. Roux and H. L. Swinney, in *Nonlinear Phenomena in Chemical Dynamics*, C. Vidal and A. Pacault, eds. Springer, New York, (1981).
- [20] As in the case of the introduction of phase, the partition of the local orbit into loops is arbitrary but the same at different points of the medium; e.g., by the semiplane  $\varphi = 0$ .
- [21] J. S. Birman, *Braids, Links and Mapping Class Groups*, Princeton Univ. Press, Princeton (1974).
- [22] We reserve the notation  $B_n$  for braids corresponding to period- $n$  orbits, while  $b_n$  denotes any braid with  $n$  threads.
- [23] A. Goryachev, H. Chaté, and R. Kapral, *Phys. Rev. Lett.*, **83**, 1878, (1999).
- [24] R. Klevecz, J. Pilliod and J. Bolen, *Chronobiology International*, **8**, 6 (1991).
- [25] L. Brunnet, H. Chaté and P. Manneville, *Physica D* **78**, 141 (1994).
- [26] A. Goryachev and R. Kapral, *Phys. Rev. Lett.*, **76**, 1619 (1996).
- [27] G. Pulignano, N. Paturno, P. Urbani, C. Greco, and G. Critelli, *Pace*, **13**, 144, (1990).

---

[1] R. Kapral and K. Showalter, eds. *Chemical Waves*